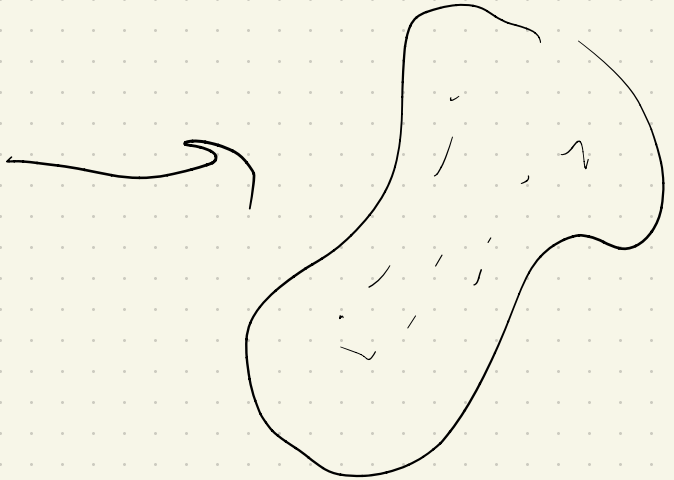
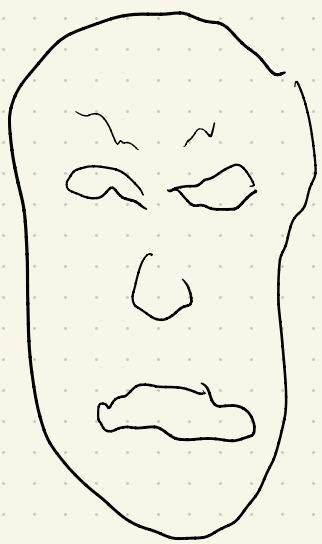


Computing Teichmüller Shape Space

Paper by Miao Jin, Wei Zeng, Feng Luo,
Xianfeng Gu

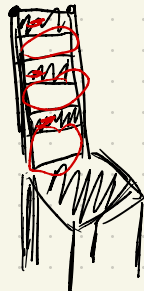
4/11/2022





Shape indexing & classification based on Conformal Geometry.

Example:



vs



Ways to think about Shape:

Topological

- Global
- succinct
- Intuitive
- less discriminatory

PH i

Differential Geometry:

- Local
- Redundant
- Much more discriminatory
- In practice, don't want to be too strict!

Conformal Maps

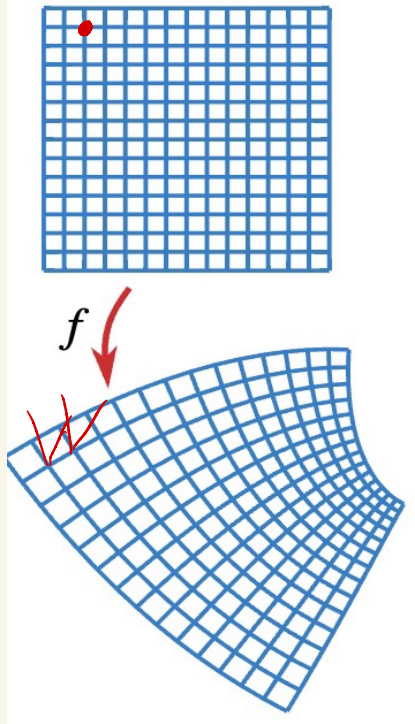
- Angle preserving map between surfaces

$f: U \rightarrow V$ is conformal at $u_0 \in U$ if it preserves
II angles between directed curves through u_0 .

2) Orientation



Eg)



Rank: Even with the same topology, two surfaces may not share a conformal map.

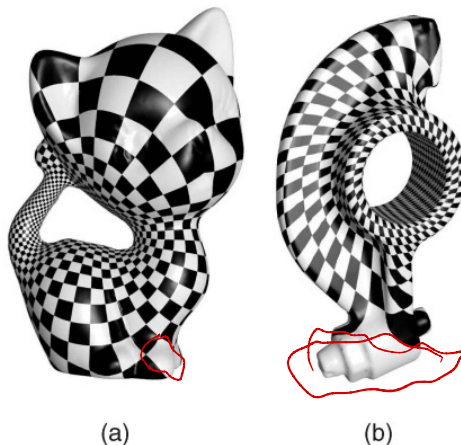
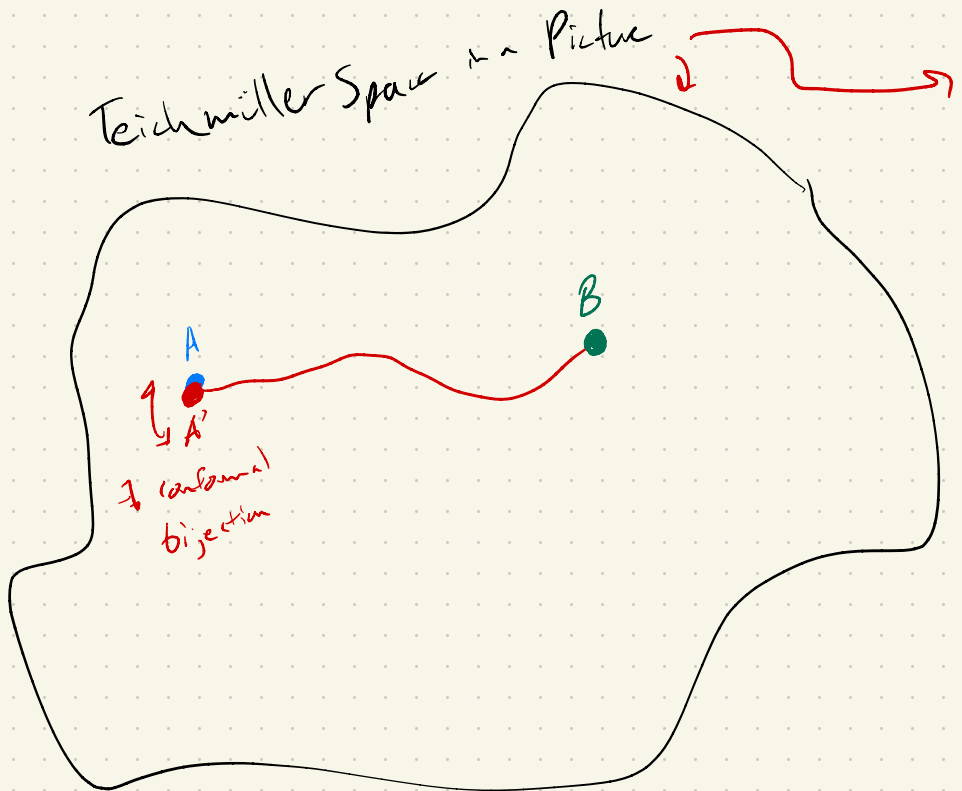


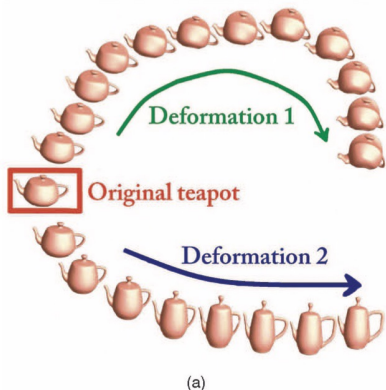
Fig. 1. A map between genus one (a) kitten model and (b) rocker-arm model, where the right corner angles on the kitten surface are distorted on the rocker-arm surface, which demonstrates that the map is not conformal.

- IF there's a bijective conformal map,
two surfaces are in same equivalence class
- All conformal classes = Teichmüller Space

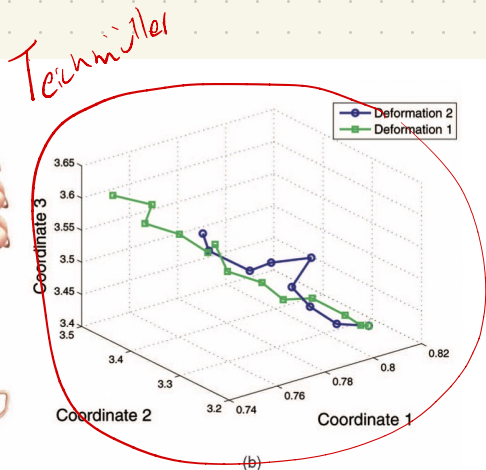
What is Teichmuller Space?

- IF there's a bijective conformal map among surfaces, we define equivalence class
- All conformal classes = Teichmuller Space





(a)

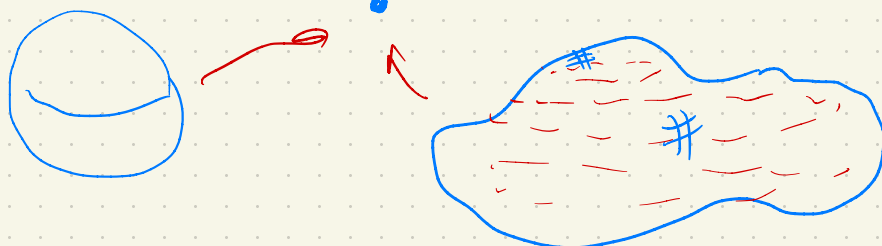


(b)

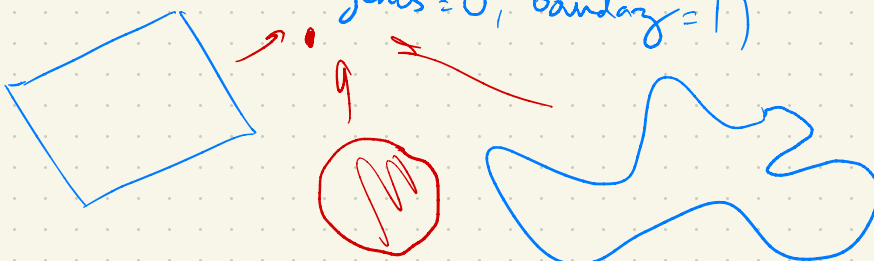
Fig. 4. The teapot surface with one handle and one boundary at the spout as shown in (a) has three dimensions in Teichmüller space, where each point represents one conformal equivalent class, and a curve connecting different points represents a deformation process from one class to the other as shown in (b). (a) Teapots deformed in euclidean space. (b) Deformation paths in Teichmüller space.

- Invariant to conformal deformations

- Teichmüller space for genus zero closed surfaces

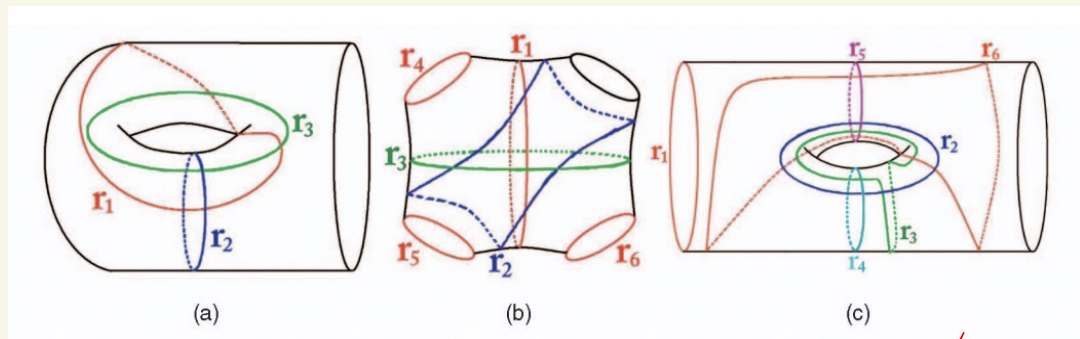


- Teichmüller space for $(0,1)$ surfaces
(genus = 0, boundary = 1)

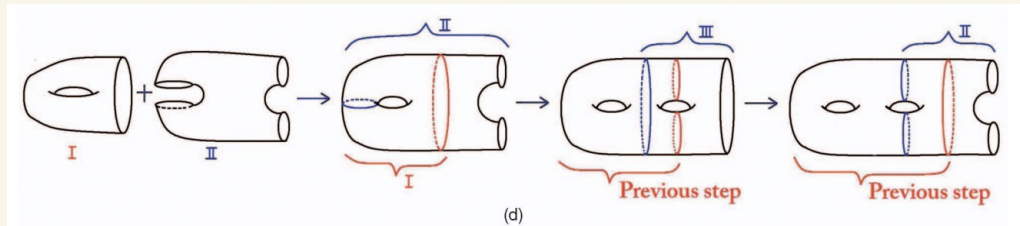


Surfaces

- Paper restricted to orientable manifolds w/ Euler characteristic ≤ 0 .
 - Given a surface $\Sigma_{g,r}$ of genus g w/ r boundaries, Σ can be built from 3 building blocks:



Eg of giving:



Can construct any surface studied in this paper by building blocks ($X(\Sigma_{g,r}) \subset O$)

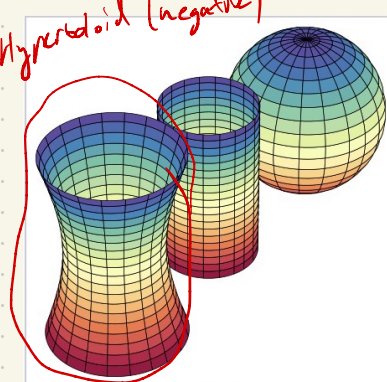
Hyperboloid Uniformization Metric

(H.U.M.)

$\Sigma \in \mathbb{R}^3$ a surface has induced Euclidean metric, \tilde{g} .

- If $u: \Sigma \rightarrow \mathbb{R}$ is a function, $e^{2u} \tilde{g}$ is a metric conformal to \tilde{g} .
- If $X(\Sigma) < 0$, $\exists \bar{g} = e^{2u} \tilde{g}$
- \bar{g} is conformal to \tilde{g}
- \bar{g} induces -1 Gaussian curvature at all interior points
+ 0 Gaussian curvature at boundary pts.

$$\bar{g} = \text{HUM}$$



Hyperbolic Geometry

Definition

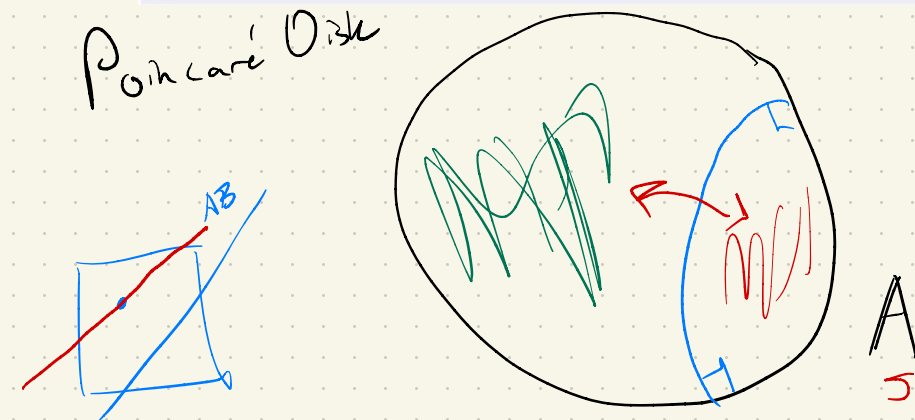
The *hyperbolic disk model* is the geometry whose points are:

$$\mathbb{H}^2 = \{(x, y) \in \mathbb{R}^2 : x^2 + y^2 < 1\}$$

The boundary circle $\mathbb{A} = \{(x, y) : x^2 + y^2 = 1\}$ is called the *absolute*. The transformation group of \mathbb{H}^2 is defined:

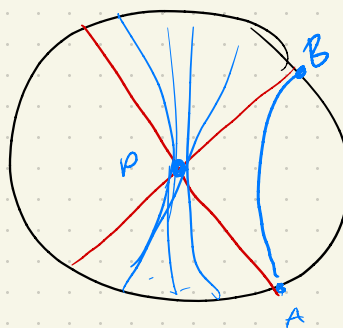
$$\mathcal{M} = \{ \text{inversions in circles orthogonal to } \mathbb{A} \}$$

Poincaré Disk



Fun facts

Euclid's 5th postulate
doesn't hold!



"Given a line AB and a point P there is a unique line l not intersecting AB "

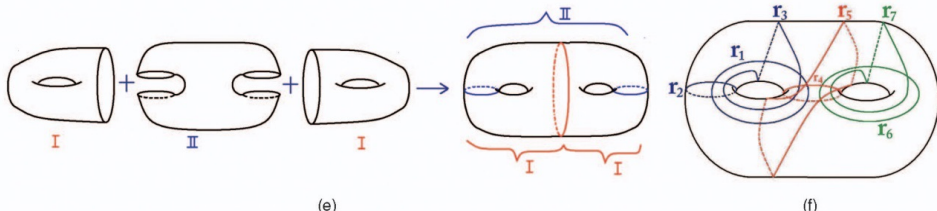


Fig. 5. (a) Building block I. (b) Building block II. (c) Building block III. For all of the three basic building blocks, the lengths of geodesic homotopic to the labeled curves determine the building block's metric. (d) Using building blocks I, II, and III to build all surfaces: from left to right, using building blocks I and II to build genus one surface with two boundaries. Then, adding building block III to build genus two surface with one boundary. Then, adding building block II to build genus two surface with two boundaries. Repeating to get all surfaces. Note that marked curves on surface indicate the boundaries of overlapping part where two building blocks are glued together, and red and blue colors are used to distinguish boundaries coming from different building blocks. (e) The construction of genus two surface. (f) The geodesic lengths of the set of color labeled curves determine the metric of a genus two surface. Blue curves and green curves come from the first and the second building blocks with type I; red curves come from building block with type II. Note that two of the curves for building block with type II and one for the second building block with type I are redundant and have been canceled off.

- Using these building blocks, we get a coordinate system in Teichmüller space
- Conformal structure is determined by geodesic lengths homotopic to red loops in figure under Hyperbolic Uniformization Metric
- For surfaces with H.U.M., the geodesic is unique in each homotopy class
(proof: Gauss-Bonnet)
- For a surface $\sum_{g \geq 1, r}$ with $\chi(\Sigma) < 0$, Teichmüller coords. are determined by

$6g + 3r - 5$ geodesics.

In a computational setting

Algos for computing Teichmüller space coords:

- coordinates represented as lengths of a special set of geodesics under H.U.M.
 - ↳ can be computed from Fuchsian transforms
 - ↳ need generators of Fuchsian groups.
 - ↳ found using system of loops.

H.U.M.

- Pipeline
- 1.) Compute hyperbolic uniformization metric of the surface (Δ-ulation)
 - 2.) Compute Fuchsian group generators
 - 3.) compute coords in Teichmüller Space

STEP 1: Computing the H.O.M.

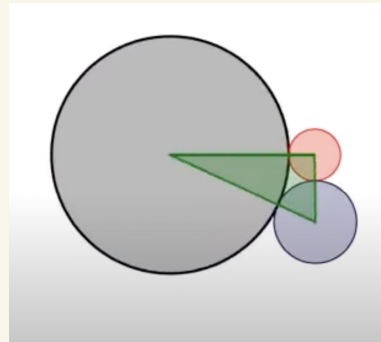
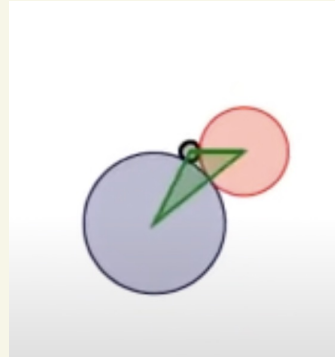
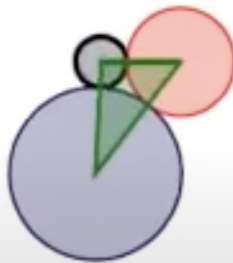
Theory: Smooth setting \rightarrow infinitesimal circles

In Practice Discrete Evaluation \rightarrow circle packing metric

- Center a cone at each vertex v_i
- Weight edge E_{ij} by intersection angle of cones centered at v_i, v_j
- Denote radius of each cone to be r_i .

Egs

2d



The Discrete Hyperbolic Surface Ricci Flow

(on a triangulation with negative Euler number)

w/ circle packing metric satisfies that
the scaling of cone radius γ_i
corresponding to $v_i \in V$ proportionally
evolves according to FL Discrete Gaussian K_i
curvature at v_i :

$$\frac{d\gamma_i}{dt} = -K_i \sinh \gamma_i$$

while intersection angles are kept unchanged.

→ final circle packing metric is conformal to original,
but introduces constantly negative Gaussian curvature.

- Converges Exponentially.
 - Namely, set initial circle packing metric,
(approximates original Euclidean metric as much as possible)
 - Use Gradient descent to solve $\frac{d\gamma_i}{dt} = -K_i \sinh \gamma_i$
- OR

- Use Newton's method:

Let $f(u) = (u_1, u_2, u_3, \dots, u_n)$, $u_0 = (0, 0, 0, \dots, 0)$
and $u_i := \ln(\tanh \frac{\gamma_i}{2})$, and $\frac{\partial f}{\partial u_i} = K_i$

$$\text{Define } f(u) = \int_{u_0}^u \sum_{i=1}^n K_i du_i,$$

Then, by design, the Ricci flow above

\Rightarrow just the negative gradient flow of conformal energy $\mathfrak{f}(u)$.

Just the solution to an energy optimization problem.

Compute Fuchsian Group Generators

- 1.) compute fundamental group generators
- 2.) isometric embed the mesh in the Poincaré disk
- 3.) compute Fuchsian group generators

* What the heck is a Fuchsian group?

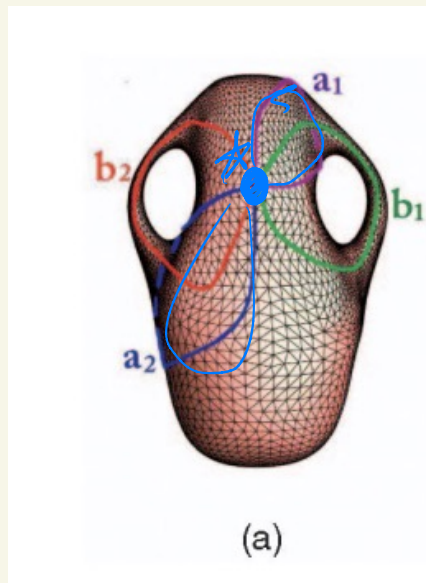
→ discrete subgroup of $PSL(2, \mathbb{R})$

group of isometries in hyperbolic plane

STEP 1: Fundamental Group generators

- pick a point on surface as base point
- for each handle, find a tunnel loop and a handle loop.
- These generate the fundamental group
↳ well studied in comp. Top.!

Example:



Base point:

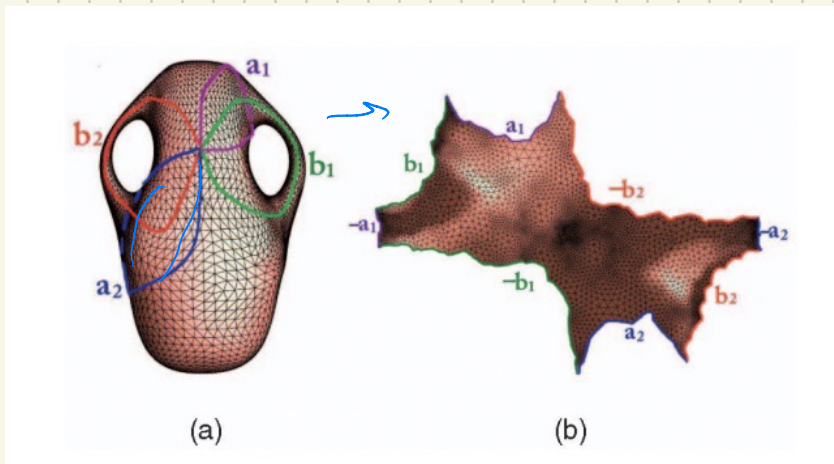
Group generators: $\{a_1, a_2, b_1, b_2\}$

Group operation?

→ slice S open along group generators
to get the "fundamental domain", a topological disk D

Embed D isometrically into Poincaré Disk

Use H.U.M. computed in step 1 to embed the mesh in Poincaré Disk



1) Pick arbitrary face $f_{012} \in D$.

Let edge lengths of $f_{012} = \{l_{01}, l_{12}, l_{20}\}$, and

corner angles of $f_{012} = \{\theta_0^{12}, \theta_1^{20}, \theta_2^{01}\}$.

2) Define $\Upsilon: D \rightarrow H^2$ for f_{012} by

$$\Upsilon(v_0) = 0 \quad \Upsilon(v_1) = \frac{e^{l_{01}} - 1}{e^{l_{01}} + 1}, \quad \Upsilon(v_2) = \frac{e^{l_{02}} - 1}{e^{l_{02}} + 1} e^{i\theta_0^{12}}$$

Möbius Transformation

3.) Embed all faces incident to $f_{0,12}$

Suppose $f_{1,2,k}$ adjacent to $f_{0,12}$.

→ $T(v_k)$ should be an intersection point of

$(T(v_1), l_{1k})$ and $(T(v_2), l_{2k})$,



so we find the intersection of corresponding hyperbolic circles in H^2 . Repeat for all f_{ijk} .

(use Hyperbolic circle \leftrightarrow Euclidean circle formula)



Fuchsian Group Generators

Let $\{a_1, b_1, \dots, a_g, b_g\}$ fundamental generators
for our mesh.

1] Möbius transformations:

$$\alpha_k : \mathbb{H}^2 \rightarrow \mathbb{H}^2, T(a_k) \rightarrow T(a_k^{-1})$$

and $\beta_k : \mathbb{H}^2 \rightarrow \mathbb{H}^2, T(b_k) \rightarrow T(b_k^{-1})$

Ex]

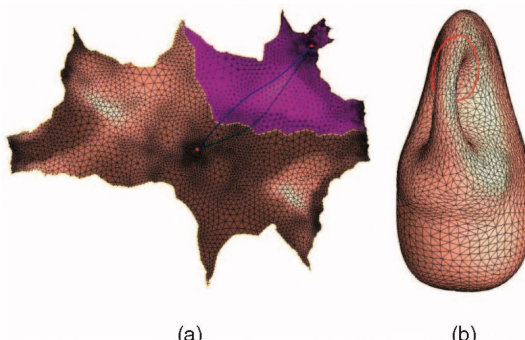


Fig. 7. (a) One deck transformation maps the left period to the right one.
(b) Two closed loops homotopic to the red one on the vase model lift as two blue paths in the universal covering space.

One possible example of a map

$$T(b_k) \rightarrow T(b_k^{-1})$$

These Möbius Transformations form the
generators of a Fuchsian group!

Details of computing B_1 :

(IF time/interest)

$$\text{Let } \mathcal{D}_T(b_1) = q_0 - p_0 \text{ and } \mathcal{D}_T(b_1^{-1}) = p_1 - q_1.$$

- Then geodesic distance from p_1, q_1 and p_0, q_0
 equal in Poincaré disk.

- To align the geodesics, construct Möbius Υ_0 ,

$$\text{where } \Upsilon_0 = e^{\frac{i\pi}{2}\Theta_0} \frac{z - p_0}{1 - \bar{p}_0 z}, \quad \Theta_0 = \arg \frac{q_0 - p_0}{1 - \bar{p}_0 q_0}$$

- $p_0 \rightarrow \text{origin}$, $q_0 \xrightarrow{\Upsilon_0} x \in \mathbb{R}^+$

- Similarly construct Υ_1 s.t.

$p_1 \xrightarrow{\Upsilon_1} \text{origin}$, $q_1 \xrightarrow{\Upsilon_1} y + i\mathbb{R}^+$, s.t.

$$\Upsilon_1(q_1) = \Upsilon_0(q_0).$$

- Then B_1 is composition: $B_1 = \Upsilon_1^{-1} \circ \Upsilon_0$ (then $p_1 = B_1(p_0)$,
 $q_1 = B_1(q_0)$)

Finally, Compute Teichmiller coords.

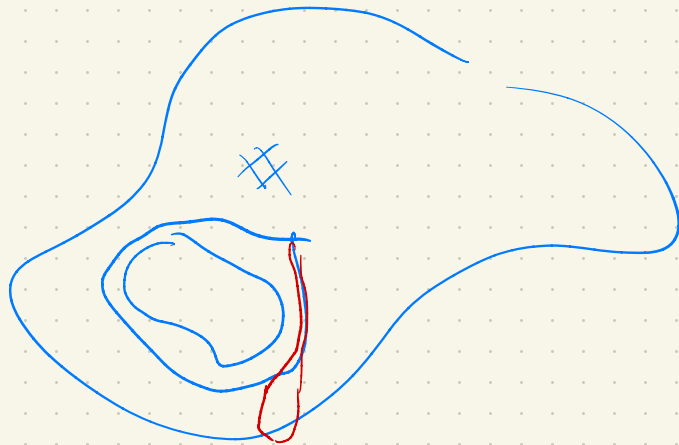
- 1) Decompose the surface to building blocks
- 2) Determine homotopy classes of geodesics
- 3) Compute length of geodesics in each homotopy class

By computing Fuchsian group generators

$\{a_1, B_1, a_2, B_2, \dots, a_g, B_g\}$ correspond to

homology basis $\{a_1, b_1, a_2, b_2, \dots, a_g, b_g\}$:

- We can compute homotopy class of any loop γ on surface (e.g.: $\gamma = a_1 b_1 a_1^{-1} b_1^{-1}$)
- Get representation w/ Fuchsian transformations by sending $a_i \rightarrow d_i$ and $b_i \rightarrow B_i$.
Then $\phi_\gamma = d_1 B_1 \cdot d_1^{-1} B_1^{-1}$
- Get length of $\gamma < l_\gamma$ by the relation:
 $| \operatorname{tr}(\phi_\gamma) | = 2 \cosh \left(\frac{l_\gamma}{2} \right)$. Done!



Fundamental a_1 , b_1



Fuchsian Möbius transforms $T(a_i) \rightarrow T(a_i^{-1})$

Computing Teichmüller Shape Space

Miao Jin, Wei Zeng, Feng Luo, and Xianfeng Gu, *Member, IEEE*

Abstract—Shape indexing, classification, and retrieval are fundamental problems in computer graphics. This work introduces a novel method for surface indexing and classification based on Teichmüller theory. Two surfaces are conformal equivalent, if there exists a bijective angle-preserving map between them. The Teichmüller space for surfaces with the same topology is a finite dimensional manifold, where each point represents a conformal equivalence class, and the conformal map is homotopic to Identity. A curve in the Teichmüller space represents a deformation process from one class to the other. In this work, we apply Teichmüller space coordinates as shape descriptors, which are succinct, discriminating and intrinsic, invariant under the rigid motions and scalings, and insensitive to resolutions. Furthermore, the method has solid theoretic foundation, and the computation of Teichmüller coordinates is practical, stable, and efficient. The algorithms for the Teichmüller coordinates of surfaces with positive or zero Euler numbers have been studied before. This work focuses on the surfaces with negative Euler numbers, which have a unique conformal Riemannian metric with -1 Gaussian curvature. The coordinates that we will compute are the lengths of a special set of geodesics under this special metric. The metric can be obtained by the curvature flow algorithm, the geodesics can be calculated using algebraic topological method. We tested our method extensively for indexing and comparison of about 100 of surfaces with various topologies, geometries, and resolutions. The experimental results show the efficacy and efficiency of the length coordinate of the Teichmüller space.

Index Terms—Surface classification, surface comparison, shape retrieval, Teichmüller space, hyperbolic structure, Fuchsian group, Ricci flow, Riemann uniformization.



1 INTRODUCTION

1.1 Motivation

EFFECTIVE index and classification for shapes are very demanding with the dramatically increasing of 3D geometric models in online repositories, while also challenging. For a geometric algorithm, all the information that can be utilized is only the *topology and geometry* of the shape. But, for human beings, shape classification and comparison involves the expectations of the *functionalities* of the objects. For example, for a human observer, the slatted chairs can still be quite similar even if they have a different number of slats; but for a computer, the objects are quite different because they have different topologies. Low-level algorithms based on the geometric information need to be developed first to lay down the foundation for high-level methods, which are closer to the human intelligence. The algorithms in both levels have fundamental importance. This work focuses on the algorithms solely based on the geometric information.

Shape descriptors can be constructed using different levels of geometric information. For example, surfaces can be classified by their topological properties, such as the

number of the handles and the boundaries. Shapes can be differentiated more precisely by differential geometric properties, such as principle curvatures and fundamental forms. Topological descriptors are global, succinct and intuitive, but less discriminating; whereas differential geometric descriptors are local, redundant, but much more discriminating. The huge storage requirements prevent differential geometric descriptors from practical applications. This work introduces a novel approach for shape indexing and classification, with descriptors based on conformal geometry. In practice, it is hard to find two different types of shapes with handles sharing the same conformal descriptors, so descriptors based on conformal geometry are discriminating enough. What is more, conformal shape descriptors are intrinsic, independent of rotation, translation, and scaling, and are also invariant to tessellation and isometric deformation. They are stable for deformations with small area stretching, like the posture change of a human skin surface, which changes slightly. They are efficient, easy to compute and compare. Therefore, we believe conformal geometric approach for shape classification and comparison has the potential for real applications.

1.2 Conformal Equivalence

A *conformal map*, also called an *angle-preserving map*, preserves local angles between two surfaces. While given two arbitrary surfaces with same topology, there may not exist conformal map between them, which is demonstrated as the angle distorted texture transferring from kitten model to rocker-arm model in Fig. 1 based on a map between them. They both are genus one surfaces, while no conformal map between them. For surfaces with the same topology, we say they are *conformally equivalent* or belong to the same conformal class if there exists a bijective conformal map between them. Therefore, surfaces can be easily differentiated by conformal

• M. Jin is with the Center for Advanced Computer Studies, University of Louisiana at Lafayette, Room 237 Computer Science and Center for Advanced Computer Studies Building, Lafayette, LA 70504.
E-mail: mjin@acs.louisiana.edu.

• W. Zeng and X. Gu are with the Department of Computer Science, Stony Brook University, Computer Science Building, Stony Brook, NY 11794.
E-mail: {zengwei, gu}@cs.sunysb.edu.

• F. Luo is with the Department of Mathematics, Rutgers University, Room 532 Hill Center-Busch Campus, 110 Frelinghuysen Road, Piscataway, NJ 08854. E-mail: fluo@math.rutgers.edu.

Manuscript received 9 July 2007; revised 22 Apr. 2008; accepted 21 Aug. 2008; published online 2 Sept. 2008.

Recommended for acceptance by C. Gotsman.

For information on obtaining reprints of this article, please send e-mail to: tvcg@computer.org, and reference IEEECS Log Number TVCG-2007-07-0080. Digital Object Identifier no. 10.1109/TVCG.2008.103.

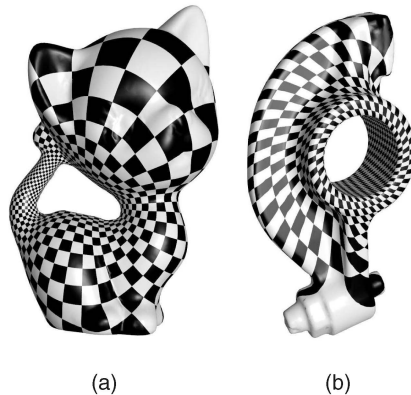


Fig. 1. A map between genus one (a) kitten model and (b) rocker-arm model, where the right corner angles on the kitten surface are distorted on the rocker-arm surface, which demonstrates that the map is not conformal.

equivalence. All conformal classes form a space called Teichmüller space, which can be modeled as a finite dimensional manifold. Each surface has a unique coordinate in the space, and the dimension of the coordinates is determined by the topology of the surface. Two surfaces share the same coordinates in Teichmüller space if and only if they belong to the same conformal class.

An intuitive example is given by two planar annuli: we can scale them such that both of their outer radii are 1, while the inner radii are r_1 and r_2 , respectively. There is no conformal map between them as long as $r_1 \neq r_2$. Therefore, the dimension of the conformal descriptors for all planar annuli is one, and the value is the inner radius after normalization. Another example is given by human faces with three boundaries in Figs. 2a, 2b, and 2c. Their conformal descriptors are the geodesic lengths of their boundaries under hyperbolic uniformization metric, after we conformally map each face to two congruent right-angled hyperbolic polygons in Poincaré disk as shown in

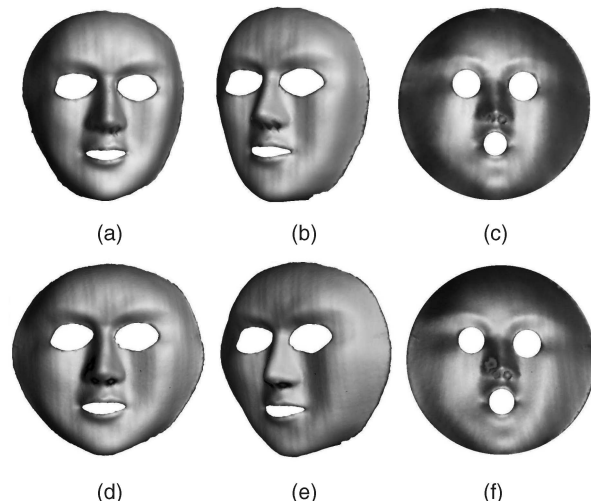


Fig. 3. Conformal descriptors are invariant under isometric deformations. The first row shows two views of the original surface and its conformal image. The second row shows two views of the deformed surface and its conformal image. Their conformal descriptors are visualized as the inner circles radii. Under isometric deformation, their conformal images are identical, which means their conformal descriptors are the same.

Figs. 2d, 2e, and 2f. The dimension of their coordinates in Teichmüller space is three, the number of boundaries. Since those edge lengths are not equal, they do not belong to the same conformal class.

Conformal descriptors are invariant under conformal deformations, which include isometric deformations, rigid motions, and scaling. Fig. 3 gives an example of a toy face (with different viewpoints in Figs. 3a and 3b) and its conformal descriptors (visualized as the three inner circles radii in Fig. 3c). After isometric deformation of the toy face (with different viewpoints in Figs. 3d and 3e), the values of its conformal descriptors (visualized as the three inner circles radii in Fig. 3f) do not change, which can be verified by the comparison of the three circles radii (between Figs. 3c and 3f), and the difference error is under 0.0177.

This work proposes to classify surfaces based on Teichmüller space theory. In this work, we only consider oriented surfaces. We use (g, r) to represent the topological type of the surface, where g means the number of handles (genus), r the number of boundaries. After fixing the topology of the surfaces, all conformally equivalent classes form a finite dimensional manifold, the so-called *Teichmüller* space [12], where each point represents conformal equivalence class, and the conformal map is homotopic to Identity. A curve connecting different points represents a deformation process from one class to the other. The dimension of the Teichmüller space of negative Euler number surfaces with topological type $(g > 1, r)$ is $6g - 5 + 3r$. Fig. 4 illustrates the concept. The teapot surface has one handle and one boundary at the spout; therefore, it is of topological type $(1, 1)$, with three dimensions in Teichmüller space. The teapot in the middle is twisted with the deformation process indicated by the blue curve. The more the curve changes, the greater the distortion is. Another deformation process is depicted by the red curve where the teapot is scaled vertically. The two deformation paths are illustrated in both \mathbb{R}^3 and the Teichmüller space.

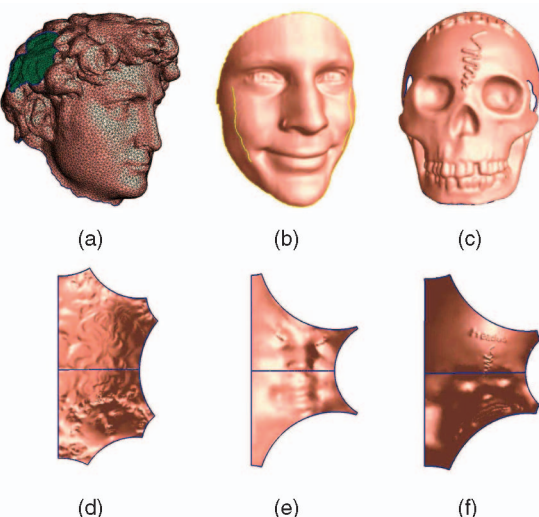


Fig. 2. Three human faces sharing the same topology (two holes annulus) are not conformally equivalent, which is verified by conformally mapping them to hyperbolic space and comparing their conformal descriptors: the edge lengths of the hyperbolic hexagon under hyperbolic uniformization metric.

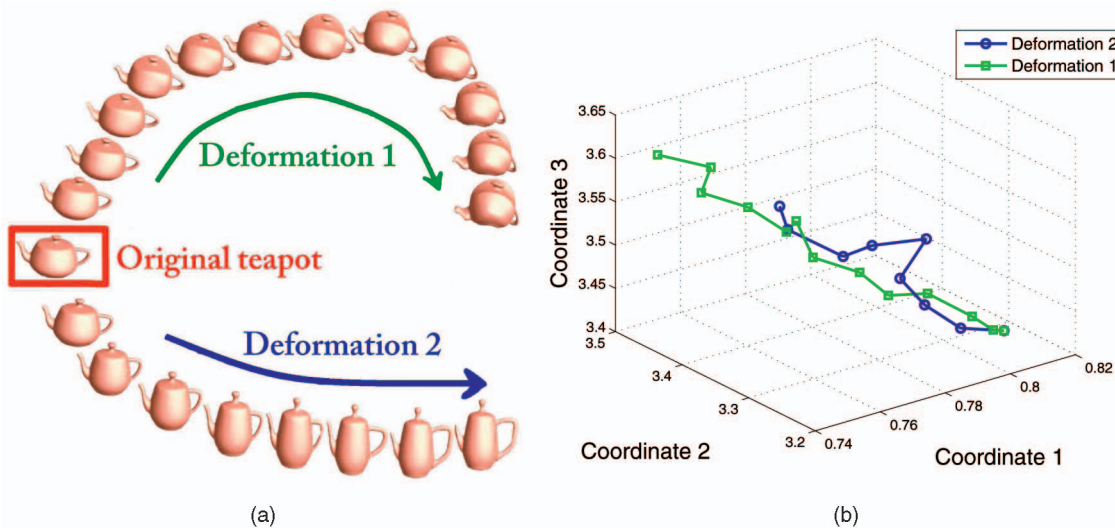


Fig. 4. The teapot surface with one handle and one boundary at the spout as shown in (a) has three dimensions in Teichmüller space, where each point represents one conformal equivalent class, and a curve connecting different points represents a deformation process from one class to the other as shown in (b). (a) Teapots deformed in Euclidean space. (b) Deformation paths in Teichmüller space.

We briefly summarize the Teichmüller spaces for surfaces with different Euler numbers. The Euler number of type (g, r) is $2 - 2g - r$. The computational algorithms for the Teichmüller coordinates of surfaces with nonnegative Euler numbers have been introduced before. This work focuses on surfaces with negative Euler numbers:

- The Teichmüller space for $(0, 0)$ type surfaces, namely genus zero closed surfaces, has only one point. That means that all genus zero closed surfaces are conformally equivalent. In this case, we conformally map the surface to the unit sphere. By mapping different surfaces to the unit sphere, we can easily construct the conformal mapping between the two surfaces. The area distortion induced by the conformal mapping is called the *conformal factor*. In [4], we proved that the conformal factor and the mean curvature determine the surface uniquely up to a rigid rotation of the sphere. We use area distortion and mean curvature as shape descriptors for shape comparison purposes in [4].
- The Teichmüller space for $(0, 1)$ type surfaces, namely genus zero surface with a single boundary, consists of a single point. All such surfaces can be mapped to the unit disk. Similarly, the conformal factor and mean curvature can be applied as shape descriptors.
- The Teichmüller space for $(1, 0)$ type surfaces, namely tori, is 2D. The Teichmüller coordinates of a torus can be computed using global surface conformal parameterization method [3]. Basically, we can compute a holomorphic 1-form. By integrating the 1-form, we can map the universal covering space of the surface to the plane \mathbb{R}^2 . Each fundamental domain is mapped to a parallelogram. The Teichmüller coordinates of the torus are the angle and the length ratio between two adjacent edges of the parallelogram. We refer readers to [3] for details.
- For all the other surfaces, the Euler numbers are negative. The coordinates in Teichmüller space can be

computed in the following method. First, there exists a unique Riemannian metric, called the *hyperbolic uniformization metric*, which is conformal to the original metric of the surface and induces -1 constant Gaussian curvature everywhere. Furthermore, all the boundaries become geodesics under the uniformization metric. Two closed curves are *homotopic*, if one can deform to the other without leaving the surface. Under the hyperbolic uniformization metric, each homotopy class has a unique geodesic. We choose a special set of homotopy classes on the surface, then compute the unique geodesic in each class. The lengths of these geodesics are Luo's coordinates [9], which form the length coordinates of the surface in Teichmüller space. This work focuses on the computation of the length coordinates of surfaces with negative Euler numbers.

The major goal of this paper is to develop rigorous and practical algorithms to compute length coordinates of surfaces with negative Euler numbers in Teichmüller space. The major contributions of this work are as follows:

1. It proposes a theoretical framework to model all negative Euler number surfaces in a shape space, Teichmüller space. The framework has deep roots in modern geometry and is practical for computation. It offers novel views and tools for tackling engineering problems.
2. It introduces a series of practical algorithms for computing length coordinates of negative Euler number surfaces in Teichmüller space. Those coordinates are with finite dimension, independent of scaling and rigid motion, and are also invariant to different tessellations. They can be applied for shape indexing to classify surfaces according to their conformal class.

The remainder of this paper is organized as follows: Section 2 contains a summary of related work, and the challenges in this area. Section 3 briefly introduces the

theoretical background of Teichmüller space. Section 4 describes our algorithms for computing the coordinates for general surfaces with negative Euler numbers in Teichmüller space. Section 5 presents results of our experiments on surface indexing and shape comparison, which evaluate the robustness, discriminability, and efficiency of our algorithms. We summarize this paper and point out future directions in Section 6.

2 RELATED WORK

Our work proposes to compute Teichmüller space coordinates as shape descriptors based on surface hyperbolic uniformization metric, which classify surfaces according to their conformal structures. Surfaces having the same descriptors share the same conformal structure, invariant to conformal deformations.

The research literature on shape descriptors is vast. A thorough review of shape descriptors is beyond the scope of the current work. We will focus here only on recent shape descriptors which are most relevant to our work using conformal geometry, and methods for designing metrics by prescribed curvatures.

2.1 Shape Descriptors

For the application of 3D shape classification and matching, shape descriptors are to extract meaningful and simplified representations from the 3D model based on the geometric and topological characteristics of the object. As the name suggests, shape descriptors should be descriptive enough to be able to discriminate similar and dissimilar shapes. The interested reader is referred to [28], [17], and [15] for comprehensive surveys of different shape descriptors and evaluations of their performance.

Shape descriptors can be classified by the corresponding transformation groups, to which they are invariant. The following transformation groups are considered: *rigid motion*, *isometric transformation*, and *conformal deformation*. The former groups are the subgroups of the latter ones. In the discussion, we focus on shape descriptors based on conformal geometry. There are many other shape descriptors invariant to the above transformation groups based on other methods. We only brief some of them.

2.1.1 Shape Descriptors Invariant to Conformal Deformations

Conformal structure is invariant to conformal deformations, which include isometric deformations and rigid motions. To the best of our knowledge, the first work proposed to use conformal structure for shape classification is [8], where the conformal structure is represented as period matrices. Later, geodesic spectra of surfaces under their uniformization metrics are applied as the conformal structure descriptors in [7], which can be computed symbolically. A general framework for 3D surface matching is proposed in [6] and [18]. By conformally parameterizing the 3D surfaces to canonical 2D domains, the matching problem is greatly simplified. If the surfaces are conformally equivalent, then 2D mapping is an identity with appropriate boundary conditions.

2.1.2 Shape Descriptors Invariant to Isometric Transformations

Pose changes are a quasi-isometric transformation of the 3D mesh, in the sense that edge lengths do not change much as a result of the transformation. Pose-invariant shape descriptors are invariant under nonrigid isometric transformations, and tolerant quasi-isometric transformations. Pose-invariant shape descriptors based on conformal geometry are introduced in [23], where the histogram of the conformal factor computed from surface uniformization metric is applied as shape descriptor. This descriptor is intrinsic and pose-invariant.

Laplace-Beltrami operator is determined by the Riemannian metric. Therefore, most descriptors related to discrete Laplace-Beltrami operators are also invariant to isometric deformations, and tolerant quasi-isometric deformations. For examples, Reuter et al. in [20] use the eigenvalues of Laplace-Beltrami operator, Rustamov in [19] uses the eigenvectors, and Xiang et al. in [21] use the histogram of the solution to the volumetric Poisson equation which involves the Laplace-Beltrami operator.

2.1.3 Shape Descriptors Invariant to Rigid Motions

Shape descriptors invariant to rigid motions and based on conformal geometry are used in [4] and [5] for medical application purpose, where both conformal factor and mean curvature are considered. Conformal factor itself fully determines the Riemannian metric of surfaces. After adding mean curvature, the two can determine the embedding of surfaces unique up to rigid motions with appropriate boundary conditions.

2.1.4 Other Shape Descriptors

There are many other shape descriptors invariant to isometric deformations based on Riemannian geometry. For example, those methods in [22], [25], and [26] compute from surface geodesic distances. The method in [27] computes the diameter of the 3D shape at each point, and the average geodesic distance from each point to all other points. The histograms of the two functions are applied as the shape descriptors.

Many global or local features based, or graph-based shape descriptors are invariant to rigid motions, while extra algorithms for feature and graph matching are necessary. We refer readers to [15] for more details.

2.2 Computing Metric from Prescribed Curvature

There are many algorithms for conformal surface parameterization in the literature. Comprehensive reviews can be found in [51] and [52]. Here, we focus on approaches to compute conformal metrics from prescribed curvatures.

Hamilton introduced Ricci flow for general Riemannian manifold in [29]. Later, Hamilton introduced surface Ricci flow in [10]. Perelman applied Ricci flow for the proof of Poincaré conjecture and Thurston's geometrization conjecture in [37], [38], and [39]. A thorough introduction to Ricci flow can be found in [30] and [31].

A circle packing algorithm was introduced by Thurston in [1]. Bowers and Hurdal [49] and Stephenson [24] improved the algorithm and built the software system.

Chow and Luo discovered the intrinsic relation between Ricci flow and circle packing and laid down the theoretic foundation for discrete Ricci flow in [11], where the existence and convergence of the discrete Ricci flow were established. The variational approach to find constant curvature metrics on triangulated surfaces was pioneered in [32], [33], and [34]. More recently, it appears in [41], [40], and [35]. Combinatorial Yamabe flow is introduced in [36].

The algorithm of discrete surface Ricci flow was given in [42], where the Ricci flows on meshes with spherical, euclidean, and hyperbolic background geometries are explained in details. Furthermore, Newton's method is directly applied to optimize the discrete Ricci energy. Optimal surface parameterization is formulated as a variational problem with respect to the target boundary curvatures in [45], and solved by constrained optimization algorithm.

Circle pattern method was proposed by Bobenko et al. in [46] and [47], which used the notion of angle structures first introduced by de Verdière [48]. Based on [46], circle pattern algorithm was introduced in [43].

Metric scaling method is introduced in [44], which solved the discretized Poisson equation with the cot-Laplace operator induced by the original metric, then use harmonic maps to compute the embedding from the result metric. The method is linear and efficient.

Similar to the formulation of combinatorial Yamabe flow introduced in [35], Springborn et al. [50] compute conformal equivalent metrics according to prescribed curvatures. The Yamabe energy in [35] is represented as an integration of a differential form, and formulated to an explicit form using Milnor's Lobachevsky function in [50]. The explicit formulas of the Hessian matrix in [35] and [50] are equivalent, which is the cot-Laplace operator.

3 TEICHMÜLLER SPACE THEORY

In this section, we briefly introduce the theoretical background of Teichmüller space theory, and the most directly related background knowledge in topology and hyperbolic geometry. For details, we refer readers to [14] for information on Algebraic topology, [13] for hyperbolic geometry, and [12] for Teichmüller space theory.

3.1 Topological Background

Let Σ be a surface, the closed curves in the surface are *homotopic* to each other if they can be deformed to each other without leaving the surface. Closed curves are classified by this homotopic relation. The homotopy classes with the same base point form a group, which is called the *fundamental group*. Suppose Σ is of genus g , then there exists a set of canonical fundamental group generators $\{a_1, b_1, a_2, b_2, \dots, a_g, b_g\}$, such that on each handle, there are two loops a_i, b_i . One loop a_i circles the hole and the other loop b_i loops around the tube. Fig. 6a shows a set of canonical fundamental group generators of a genus two surface.

Suppose $\bar{\Sigma}$ is another surface, then $(\bar{\Sigma}, \pi)$ is said to be a *covering space* of Σ if locally, π is a homeomorphism. If $\bar{\Sigma}$ is simply connected, then $(\bar{\Sigma}, \pi)$ is the *universal covering space* of Σ .

For surface with negative Euler number, its universal covering space $\bar{\Sigma}$ is the hyperbolic space \mathbb{H}^2 , which will be introduced in Section 3.3. Its *Fuchsian transformations*, the transformations of the universal covering space to itself, $\phi : \bar{\Sigma} \rightarrow \bar{\Sigma}$, are hyperbolic rigid motions (Möbius transformations). Each Fuchsian transformation associates a homotopy class in the fundamental group in the following manner: giving a point p on Σ and $\bar{p}_0, \bar{p}_1 \in \pi^{-1}(p)$ on the universal covering space $\bar{\Sigma}$. If ϕ is a Fuchsian transformation, such that $\phi(\bar{p}_0) = \bar{p}_1$, then any path $\bar{\gamma} \subset \bar{\Sigma}$ connecting \bar{p}_0 and \bar{p}_1 will be projected to a closed curve $\gamma = \pi(\bar{\gamma})$. Then, we associate ϕ with the homotopy class of γ . Therefore, the Fuchsian transformation group is isotopic to the fundamental group of the surface.

3.2 Hyperbolic Uniformization Metric

A surface Σ in \mathbb{R}^3 has an induced euclidean metric, denoted as g . Suppose u is a function defined on Σ , $u : \Sigma \rightarrow \mathbb{R}$, then $e^{2u}g$ is another metric conformal to the original one. If Σ has a negative Euler number, then it has a unique metric $\bar{g} = e^{2\bar{u}}g$, which is conformal to g and induces -1 Gaussian curvature at all interior points and 0 geodesic curvature at boundary points. The metric \bar{g} is called the *hyperbolic uniformization metric* of Σ .

In order to compute the hyperbolic uniformization metric, we need to find the function $\bar{u} : \Sigma \rightarrow \mathbb{R}$, which can be solved using *Ricci flow method*:

$$\frac{du(t)}{dt} = -2K(t), u(0) = 0,$$

where $K(t)$ is induced by the metric of $e^{2u(t)}g$. It has been proven that Ricci flow will converge $u(0) = 0$ to $u(\infty) = \bar{u}$ which induces the hyperbolic uniformization metric [10].

3.3 Hyperbolic Geometry

If Σ has a negative Euler number, then with uniformization metric, the universal covering space $\bar{\Sigma}$ can be isometrically embedded in the hyperbolic space \mathbb{H}^2 .

There are two commonly used models for hyperbolic space, the *Poincaré disk* and the *upper half plane model*. The Poincaré disk is the unit disk in the complex plane, $|z| < 1$, with Riemannian metric $ds^2 = \frac{dzd\bar{z}}{(1-z\bar{z})^2}$. The rigid motions are the so-called *Möbius transformations* with the form $w = e^{i\theta} \frac{z-z_0}{1-\bar{z}_0z}$. The hyperbolic lines are circular arcs perpendicular to the unit circle. The second model is the upper half plane model $y > 0$ with the metric $ds^2 = \frac{dzd\bar{z}}{y^2}$. The Möbius motions are of the form

$$w = \frac{az+b}{cz+d}, a, b, c, d \in \mathbb{R}, ad - bc = 1.$$

A Möbius transformation in the upper half plane model is represented by its coefficient matrix. The coefficient matrix of the product of two Möbius transformations is equal to the product of their coefficient matrices.

The conformal transformation that maps the upper half plane to the Poincaré disk is $T = \frac{i-z}{i+z}$. Any Möbius

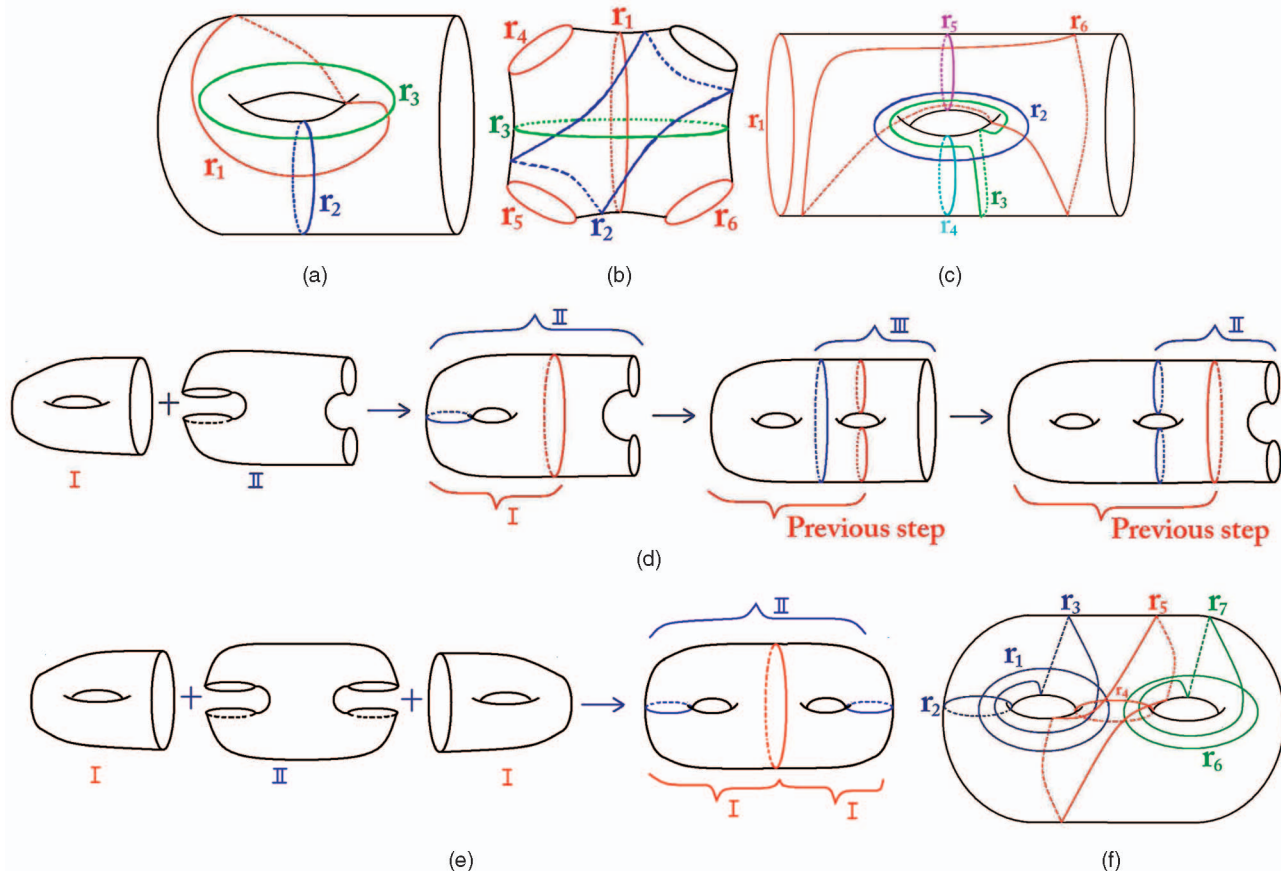


Fig. 5. (a) Building block I. (b) Building block II. (c) Building block III. For all of the three basic building blocks, the lengths of geodesic homotopic to the labeled curves determine the building block's metric. (d) Using building blocks I, II, and III to build all surfaces: from left to right, using building blocks I and II to build genus one surface with two boundaries. Then, adding building block III to build genus two surface with one boundary. Then, adding building block II to build genus two surface with two boundaries. Repeating to get all surfaces. Note that marked curves on surface indicate the boundaries of overlapping part where two building blocks are glued together, and red and blue colors are used to distinguish boundaries coming from different building blocks. (e) The construction of genus two surface. (f) The geodesic lengths of the set of color labeled curves determine the metric of a genus two surface. Blue curves and green curves come from the first and the second building blocks with type I; red curves come from building block with type II. Note that two of the curves for building block with type II and one for the second building block with type I are redundant and have been canceled off.

transformation on the Poincaré disk ϕ can be converted to a Möbius transformation on the upper half plane as

$$T^{-1} \circ \phi \circ T. \quad (1)$$

The deck transformations of $\bar{\Sigma}$ on the hyperbolic disk are Möbius transformations, which form the *Fuchsian group* of Σ . Corresponding to the canonical fundamental group generators $\{a_1, b_1, a_2, b_2, \dots, a_g, b_g\}$, the canonical Fuchsian group generators are referred as $\{\alpha_1, \beta_1, \alpha_2, \beta_2, \dots, \alpha_g, \beta_g\}$. Suppose a loop has homotopy class $a_i b_j$, then its corresponding Fuchsian transformation is $\alpha_i \circ \beta_j$.

Suppose γ is a closed curve on a surface Σ with the hyperbolic uniformization metric, then there is a unique geodesic $\tilde{\gamma}$ homotopic to γ . Also, there is a unique Fuchsian transformation ϕ associated with the homotopy class of γ . The length of $\tilde{\gamma}$, $l(\tilde{\gamma})$, satisfies the following equation:

$$|trace(\phi)| = 2 \cosh\left(\frac{l(\tilde{\gamma})}{2}\right).$$

In our implementation, we use this relation to compute the lengths of geodesics which are homotopic to a set of special closed loops on surfaces.

3.4 Teichmüller Space Coordinates

There are several coordinates defined in Teichmüller space. Here, we adopt Luo's coordinates in [9] to avoid complicated computation of the twisting angles of Fenchel-Nielsen coordinates in [12].

In the following discussion, we use $\Sigma_{g,r}$ to represent a surface Σ with topological type (g, r) , where g represents the genus, r means the number of boundaries.

Given a surface $\Sigma_{g,r}$ with negative Euler number, we can decompose the surface into three types of building blocks, as shown in Figs. 5a, 5b, and 5c. The procedure to build Σ from the building blocks is illustrated in Fig. 5d. We use $I \cap II$ to denote the process of gluing the block I to the block II . The gluing does not mean combining two blocks along their corresponding boundary curves, but by merging their overlapping regions. For example, in the first gluing step in the figure, the overlapping region of I and II is a two-holed annulus. From left to right, we use basic building blocks I and II so that $I \cap II$ is homeomorphic to $\Sigma_{1,2}$, a genus one surface with two boundaries; smoothly joining building block III , so that $\Sigma_{1,2} \cap III$ is homeomorphic to $\Sigma_{2,1}$, a genus two surface with one boundary; then joining building block II , so that $\Sigma_{2,1} \cap II$ is homeomorphic to $\Sigma_{2,2}$, a genus two surface with

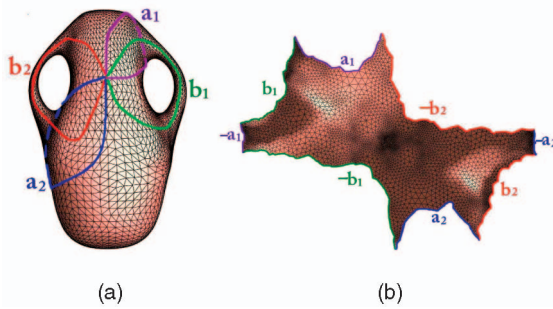


Fig. 6. (a) Vase model with a set of canonical fundamental group generators marked with red. (b) Fundamental domain of the vase model embedded in the Poincaré disk with the hyperbolic uniformization metric.

two boundaries; repeating this procedure, we can generate all types of surfaces with negative Euler surfaces. By this construction, a simple method is provided to define Luo's coordinates in Teichmüller space for general surfaces.

For each building block, its conformal structure is determined by the lengths of geodesic homotopic to those red loops under the hyperbolic uniformization metric.

Although on general surfaces, in each homotopy class, there may be multiple geodesics, which are the locally shortest curves on surfaces. For surfaces with hyperbolic uniformization metric, the geodesic is unique in each homotopy class, which can be proved by Gauss-Bonnet theorem. We refer readers to [2] for details.

When two building blocks are glued together to form a new surface, nonhomotopic loops on the original blocks may become homotopic on the resulting surface. After canceling off the redundant loops, the lengths of geodesic homotopic to remaining loops determine the conformal structure of the resulting surface, which are the coordinates of this surface in Teichmüller space. For example, for a closed genus two surface, constructed from two building blocks of type I and one building block of type II as shown in Fig. 5e, its Teichmüller coordinates are the lengths of geodesic homotopic to those loops marked with different colors as shown in Fig. 5f. Loops with the same color indicate that they come from the same building block. In general, for a surface $\Sigma_{g>1,r}$ with a negative Euler number, their Teichmüller coordinates are determined by the lengths of $6g + 3r - 5$ closed geodesics.

4 ALGORITHMS TO COMPUTE LENGTH COORDINATES IN TEICHMÜLLER SPACE

This section explains the algorithms for computing the Teichmüller space coordinates for surfaces with negative Euler numbers in details, represented as the lengths of a special set of geodesics under hyperbolic uniformization metric. The lengths of those geodesics can be symbolically computed from Fuchsian transformations, which require the generators of Fuchsian group, and Fuchsian group generators are calculated using the system of loops: canonical fundamental group generators. All of these computations are based on hyperbolic geometry.

The whole algorithm pipeline is as follows:

1. compute hyperbolic uniformization metric of the surface, discussed in Section 4.1;

2. compute Fuchsian group generators, discussed in Section 4.2; and
3. compute the coordinates in Teichmüller space, discussed in Section 4.3.

Following this pipeline, we discuss each step in detail.

4.1 Step 1. Compute Hyperbolic Uniformization Metric

In engineering fields, smooth surfaces are often approximated by discrete surfaces with triangulations. Since conformal deformation transforms infinitesimal circles to other infinitesimal circles and preserves the intersection angles among the circles, we can approximate discrete conformal deformation using circle packing metric introduced by Thurston in [1] by associating each vertex v_i with a cone of radius γ_i , each edge with edge weight Phi_{ij} which is the intersection angle of the two cones centered with the ending vertices v_i and v_j of that edge e_{ij} .

The discrete hyperbolic surface Ricci flow on a discrete negative Euler number surface with circle packing metric is a process that the scaling of cone radius of Vertex v_i is proportionally evolving according to the discrete Gaussian curvature K_i of that vertex:

$$\frac{d\gamma_i}{dt} = -K_i \sinh \gamma_i, \quad (2)$$

while the intersection angles Φ_{ij} are kept unchanged. The final circle packing metric induces new metric of original surface approximated by edge lengths, which is conformal to the original one but induces constantly negative Gaussian curvature, called hyperbolic uniformization metric. The discrete hyperbolic Ricci flow will converge exponentially. We refer the readers to [11] for theoretical proofs for the convergence of the discrete hyperbolic Ricci flow.

To compute discrete hyperbolic Ricci flow, we need to set the initial circle packing metric for a given discrete surface, which approximates its original euclidean metric as much as possible. Then, we can use gradient descent method to solve (2). The detailed algorithm can be found in Appendix Algorithm 1.

We can further improve the convergence speed of computing discrete hyperbolic Ricci flow with Newton's method. Let $u_i = \ln \tanh \frac{\gamma_i}{2}$, we can define an energy form

$$f(\mathbf{u}) = \int_{\mathbf{u}_0}^{\mathbf{u}} \sum_{i=1}^n K_i du_i,$$

where $\mathbf{u} = (u_1, u_2, \dots, u_n)$, $\mathbf{u}_0 = (0, 0, \dots, 0)$ and $\frac{\partial f}{\partial u_i} = K_i$. Then, the discrete hyperbolic surface Ricci flow in (2) is the negative gradient flow of this convex energy $f(\mathbf{u})$, and the solution of an energy optimization problem. So, in practice, we can use Newton's method to compute hyperbolic uniform metric with even faster convergence speed.

4.2 Step 2. Compute Fuchsian Group Generators in the Poincaré Disk Model

This step aims to compute the canonical Fuchsian group generators used for computing the geodesic lengths in the future step. There are several major steps to compute Fuchsian group generators:

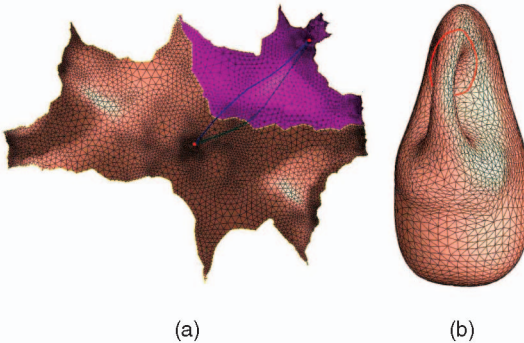


Fig. 7. (a) One deck transformation maps the left period to the right one. (b) Two closed loops homotopic to the red one on the vase model lift as two blue paths in the universal covering space.

1. compute fundamental group generators, discussed in Section 4.2.1;
2. isometric embed the mesh in the Poincaré disk, discussed in Section 4.2.2; and
3. compute the Fuchsian group generators, discussed in Section 4.2.3.

4.2.1 Compute Fundamental Group Generators

On a “marked” surface, which means we have enumerated surface handles with h_1, h_2, h_3 , etc., we pick a point on the surface as the base point (which can be any vertex on the surface), then for each handle h_i , we can uniquely decide a tunnel loop a_i which goes around the circle, a handle loop b_i which goes around the handle, and both of them go through the base point. In this way, we get a set of canonical fundamental group generators $\{a_1, b_1, a_2, b_2, \dots, a_g, b_g\}$. Fig. 6a shows a set of canonical fundamental group generators marked with different colors on the vase model. The way to compute the canonical fundamental group generators has been studied in computational topology and computer graphics literature. We adopted the methods introduced in [16]. The surface S is then sliced open along the fundamental group generators to form a topological disk D , called fundamental domain. The boundary of D takes the form $\partial D = a_1 b_1 a_1^{-1} b_1^{-1} a_2 b_2 a_2^{-1} b_2^{-1} \dots a_g b_g a_g^{-1} b_g^{-1}$.

4.2.2 Isometric Embedding in Hyperbolic Disk

Now, we isometrically embed D onto the Poincaré disk using the uniformization metric computed from the first step. Let $\tau : D \rightarrow \mathbb{H}^2$ denote the isometric embedding.

First, we select an arbitrary face f_{012} from D as a starting face. Suppose the three edge lengths of the face are $\{l_{01}, l_{12}, l_{20}\}$, and the corner angles are $\{\theta_0^{12}, \theta_1^{20}, \theta_2^{01}\}$ under the uniform hyperbolic metric. We can simply embed the triangle as

$$\tau(v_0) = 0, \tau(v_1) = \frac{e^{l_{01}} - 1}{e^{l_{01}} + 1}, \tau(v_2) = \frac{e^{l_{02}} - 1}{e^{l_{02}} + 1} e^{i\theta_0^{12}}.$$

Second, we can embed all the faces which share an edge with the starting face. Suppose a face f_{ijk} is adjacent to the starting face, and vertices v_i and v_j have been embedded. A hyperbolic circle is denoted as (c, r) , where c is the center and r is the radius. Then, $\tau(v_k)$ should be one of the two intersection points of $(\tau(v_i), l_{ik})$ and $(\tau(v_j), l_{jk})$. Also, the

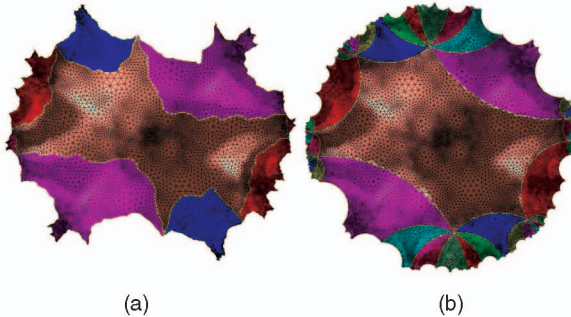


Fig. 8. (a) $2g$ Fuchsian group generators act on the vase model, which are rigid motions in the hyperbolic space. Different color indicates different periods (fundamental domains). The generators map the central period to the colored ones, respectively. (b) A finite portion of the universal covering space of the vase model generated by the actions of Fuchsian group elements with boundaries marked with geodesics in hyperbolic space.

orientation of $\tau(v_i), \tau(v_j), \tau(v_k)$ should be counterclockwise. In the Poincaré model, a hyperbolic circle (c, r) coincides with a Euclidean circle (C, R) :

$$C = \frac{2 - 2\mu^2}{1 - \mu^2|c|^2} c, \quad R^2 = |C|^2 - \frac{|c|^2 - \mu^2}{1 - \mu^2|c|^2},$$

where $\mu = \frac{e^r - 1}{e^r + 1}$. The intersection points between two hyperbolic circles can be found by intersecting the corresponding Euclidean circles. The orientation of triangles can also be determined using Euclidean geometry on the Poincaré disk.

Then, we can continue to embed faces which share edges with embedded faces in the same manner, until we embed the whole D onto the Poincaré disk.

Fig. 6b shows the embedding of fundamental domain of the vase model onto the Poincaré disk with its hyperbolic uniformization metric.

4.2.3 Fuchsian Group Generators

The embedding of a canonical fundamental domain for a closed genus g surface has $4g$ different sides, which induce $4g$ rigid transformations. These $4g$ rigid motions are the Fuchsian group generators.

Figs. 6, 7, and 8 illustrate the process to compute Fuchsian group generators for a mesh with a negative Euler number. Let $\{a_1, b_1, \dots, a_g, b_g\}$ be a set of canonical fundamental group generators as marked with red in Fig. 6a, where g is the genus. The embedding of the vase’s canonical fundamental domain in hyperbolic space has $4g$ sides, $\tau(a_1), \tau(b_1), \tau(a_1^{-1}), \tau(b_1^{-1}), \dots, \tau(a_g), \tau(b_g), \tau(a_g^{-1}), \tau(b_g^{-1})$ (see Fig. 6b in Poincaré disk). There exists unique Möbius transformations α_k, β_k , which map the $\tau(a_k)$ and $\tau(b_k)$ to $\tau(a_k^{-1})$ and $\tau(b_k^{-1})$, respectively. Fig. 7a shows one Fuchsian group generator acting on one copy of the fundamental domain of the vase model, which maps the $\tau(b_k)$ to $\tau(b_k^{-1})$. The two red points are the preimages of a same point on the vase model. Paths connecting them are projected to closed loops homotopic to the red one on the vase model (see Fig. 7b). And we will see that the computation of the length of the geodesic homotopy to the loop in Fig. 7b only involves the Möbius transformation which maps $\tau(b_k)$ to $\tau(b_k^{-1})$. The Möbius transformations $\{\alpha_1, \beta_1, \alpha_2, \beta_2, \dots, \alpha_g, \beta_g\}$ form a set

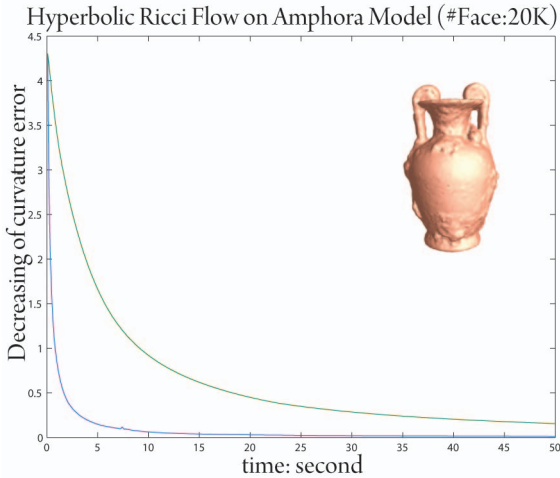


Fig. 9. Performance of curvature flow to compute hyperbolic uniformization metric for closed genus two amphora model with 20k faces. The horizontal axis represents time, and the vertical axis represents the maximal curvature error. The blue curves are for the Newton's method; the green curves are for the gradient descent method. The tests were carried out on a laptop with 1.7-GHz CPU and 1-Gbyte RAM. All the algorithms are written in C++ on a Windows platform without using any other numerical library.

of generators of Fuchsian group. Fig. 8a shows eight copies of the fundamental domain of the vase model tessellated coherently along boundaries by a set of Fuchsian group generators, and Fig. 8b shows more copies tessellated by Fuchsian transformations.

The following explains the details for computing β_1 . Let the starting and ending vertices of the two sides be $\partial\tau(b_1) = q_0 - p_0$ and $\partial\tau(b_1^{-1}) = p_1 - q_1$. Then, the geodesic distance from p_0 to q_0 equals to the geodesic distance from p_1 to q_1 in the Poincaré disk. To align them, we first construct a Möbius transformation τ_0 , which maps p_0 to the origin, and q_0 to a positive real number, with

$$\tau_0 = e^{-i\theta_0} \frac{z - p_0}{1 - \bar{p}_0 z}, \quad \theta_0 = \arg \frac{q_0 - p_0}{1 - \bar{p}_0 q_0}.$$

Similarly, we can construct another Möbius transformation τ_1 , which maps p_1 to the origin, and q_1 to a real number, with $\tau_1(q_1)$ equals to $\tau_0(q_0)$. By composing the two, we get the final Möbius transformation $\beta_1 = \tau_1^{-1} \circ \tau_0$, which satisfies $p_1 = \beta_1(p_0)$ and $q_1 = \beta_1(q_0)$, and aligns the two sides together.

Then, we convert the Fuchsian group generators from the Poincaré disk model to the upper half plane model using formula 1.

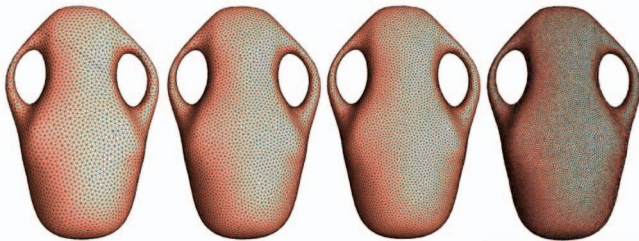


Fig. 10. Same model with different triangulation density: 5k, 10k, 20k, and 40k. Comparison of Teichmüller space coordinates with different densities is listed in Table 1.

TABLE 1
Comparison of Coordinates of Vase Model with Different Densities

Vase Model	Coordinates of Vase Model						
	1st	2nd	3rd	4th	5th	6th	7th
Face #: 5k	3.55027	0.99990	3.88055	5.55885	6.11438	3.33029	3.66071
Face #: 10k	3.55700	0.99832	3.88144	5.55611	6.11180	3.33369	3.66703
Face #: 20k	3.55805	0.99759	3.88316	5.55517	6.11112	3.33357	3.66713
Face #: 40k	3.55905	0.99559	3.88416	5.55417	6.11012	3.33367	3.66813
Average	3.55609	0.99785	3.88232	5.55607	6.11185	3.33280	3.66575
Std. Dev.	0.00343	0.00154	0.00141	0.00174	0.00157	0.00145	0.00294

The dimension of Teichmüller space coordinates for closed genus two surfaces is seven.

4.3 Compute Teichmüller Coordinates

Teichmüller coordinates are obtained by measuring the lengths of geodesic homotopic to a group of loops on surfaces under hyperbolic uniformization metric, and the geodesics are unique in each homotopy class since Gauss curvature is constantly negative everywhere. The major steps are as follows:

1. Decompose the surface to building blocks.
2. Determine the homotopy classes of the geodesics.
3. Compute the lengths of the geodesics in each homotopy class.

Surface with enumerated handles has fixed decomposition to building blocks with one handle by one handle as illustrated inversely in Fig. 4d since the decomposition is purely based on topology. After redundant loops with the same homotopic class while belonging to different building blocks have been removed, our goal is to compute the lengths of geodesic homotopic to the remaining loops. For example, for a genus two surface, the remaining loops can be seen in Fig. 5f.

Since in the above steps, the canonical homology basis $\{a_1, b_1, a_2, b_2, \dots, a_g, b_g\}$ and the corresponding Fuchsian group generator $\{\alpha_1, \beta_1, \alpha_2, \beta_2, \dots, \alpha_g, \beta_g\}$ have been calculated already. To compute the length of geodesic homotopic to a loop γ on surface, we first use the algorithm in [14] to determine its homotopy class, which can be symbolically

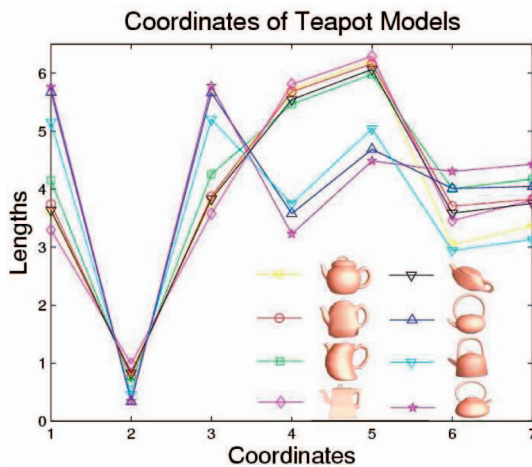


Fig. 11. The dimension of Teichmüller space coordinates for closed genus two surfaces is seven. Here, we visualize the Teichmüller space coordinates for teapots listed in Table 3.

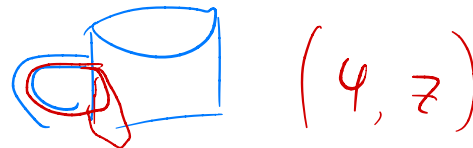


TABLE 2
Distances between Genus Two Surfaces in Teichmüller Space

distance	1	2	3	4	5	6	7	8	9	10	11	12	13	14	15	16	17	18	19	20	21	22	23	24	25	26	27	28	29	30	31	32	33	34	35	36	37	38	39	40	41	42	43	44	45	46	47	48	49	50	51	52	53	54	55	56	57	58	59	60	61	62	63	64	65	66	67	68	69	70	71	72	73	74	75	76	77	78	79	80	81	82	83	84	85	86	87	88	89	90	91	92	93	94	95	96	97	98	99	100	101	102	103	104	105	106	107	108	109	110	111	112	113	114	115	116	117	118	119	120	121	122	123	124	125	126	127	128	129	130	131	132	133	134	135	136	137	138	139	140	141	142	143	144	145	146	147	148	149	150	151	152	153	154	155	156	157	158	159	160	161	162	163	164	165	166	167	168	169	170	171	172	173	174	175	176	177	178	179	180	181	182	183	184	185	186	187	188	189	190	191	192	193	194	195	196	197	198	199	200	201	202	203	204	205	206	207	208	209	210	211	212	213	214	215	216	217	218	219	220	221	222	223	224	225	226	227	228	229	230	231	232	233	234	235	236	237	238	239	240	241	242	243	244	245	246	247	248	249	250	251	252	253	254	255	256	257	258	259	260	261	262	263	264	265	266	267	268	269	270	271	272	273	274	275	276	277	278	279	280	281	282	283	284	285	286	287	288	289	290	291	292	293	294	295	296	297	298	299	300	301	302	303	304	305	306	307	308	309	310	311	312	313	314	315	316	317	318	319	320	321	322	323	324	325	326	327	328	329	330	331	332	333	334	335	336	337	338	339	340	341	342	343	344	345	346	347	348	349	350	351	352	353	354	355	356	357	358	359	360	361	362	363	364	365	366	367	368	369	370	371	372	373	374	375	376	377	378	379	380	381	382	383	384	385	386	387	388	389	390	391	392	393	394	395	396	397	398	399	400	401	402	403	404	405	406	407	408	409	410	411	412	413	414	415	416	417	418	419	420	421	422	423	424	425	426	427	428	429	430	431	432	433	434	435	436	437	438	439	440	441	442	443	444	445	446	447	448	449	450	451	452	453	454	455	456	457	458	459	460	461	462	463	464	465	466	467	468	469	470	471	472	473	474	475	476	477	478	479	480	481	482	483	484	485	486	487	488	489	490	491	492	493	494	495	496	497	498	499	500	501	502	503	504	505	506	507	508	509	510	511	512	513	514	515	516	517	518	519	520	521	522	523	524	525	526	527	528	529	530	531	532	533	534	535	536	537	538	539	540	541	542	543	544	545	546	547	548	549	550	551	552	553	554	555	556	557	558	559	560	561	562	563	564	565	566	567	568	569	570	571	572	573	574	575	576	577	578	579	580	581	582	583	584	585	586	587	588	589	590	591	592	593	594	595	596	597	598	599	600	601	602	603	604	605	606	607	608	609	610	611	612	613	614	615	616	617	618	619	620	621	622	623	624	625	626	627	628	629	630	631	632	633	634	635	636	637	638	639	640	641	642	643	644	645	646	647	648	649	650	651	652	653	654	655	656	657	658	659	660	661	662	663	664	665	666	667	668	669	670	671	672	673	674	675	676	677	678	679	680	681	682	683	684	685	686	687	688	689	690	691	692	693	694	695	696	697	698	699	700	701	702	703	704	705	706	707	708	709	710	711	712	713	714	715	716	717	718	719	720	721	722	723	724	725	726	727	728	729	730	731	732	733	734	735	736	737	738	739	740	741	742	743	744	745	746	747	748	749	750	751	752	753	754	755	756	757	758	759	760	761	762	763	764	765	766	767	768	769	770	771	772	773	774	775	776	777	778	779	780	781	782	783	784	785	786	787	788	789	790	791	792	793	794	795	796	797	798	799	800	801	802	803	804	805	806	807	808	809	810	811	812	813	814	815	816	817	818	819	820	821	822	823	824	825	826	827	828	829	830	831	832	833	834	835	836	837	838	839	840	841	842	843	844	845	846	847	848	849	850	851	852	853	854	855	856	857	858	859	860	861	862	863	864	865	866	867	868	869	870	871	872	873	874	875	876	877	878	879	880	881	882	883	884	885	886	887	888	889	890	891	892	893	894	895	896	897	898	899	900	901	902	903	904	905	906	907	908	909	910	911	912	913	914	915	916	917	918	919	920	921	922	923	924	925	926	927	928	929	930	931	932	933	934	935	936	937	938	939	940	941	942	943	944	945	946	947	948	949	950	951	952	953	954	955	956	957	958	959	960	961	962	963	964	965	966	967	968	969	970	971	972	973	974	975	976	977	978	979	980	981	982	983	984	985	986	987	988	989	990	991	992	993	994	995	996	997	998	999	1000	1001	1002	1003	1004	1005	1006	1007	1008	1009	10010	10011	10012	10013	10014	10015	10016	10017	10018	10019	10020	10021	10022	10023	10024	10025	10026	10027	10028	10029	10030	10031	10032	10033	10034	10035	10036	10037	10038	10039	10040	10041	10042	10043	10044	10045	10046	10047	10048	10049	10050	10051	10052	10053	10054	10055	10056	10057	10058	10059	10060	10061	10062	10063	10064	10065	10066	10067	10068	10069	10070	10071	10072	10073	10074	10075	10076	10077	10078	10079	10080	10081	10082	10083	10084	10085	10086	10087	10088	10089	10090	10091	10092	10093	10094	10095	10096	10097	10098	10099	100100	100101	100102	100103	100104	100105	100106	100107	100108	100109	100110	100111	100112	100113	100114	100115	100116	100117	100118	100119	100120	100121	100122	100123	100124	100125	100126	100127	100128	100129	100130	100131	100132	100133	100134	100135	100136	100137	100138	100139	100140	100141	100142	100143	100144	100145	100146	100147	100148	100149	100150	100151	100152	100153	100154	100155	100156	100157	100158	100159	100160	100161	100162	100163	100164	100165	100166	100167	100168	100169	100170	100171	100172	100173	100174	100175	100176	100177	100178	100179	100180	100181	100182	100183	100184	100185	100186	100187	100188	100189	100190	100191	100192	100193	100194	100195	100196	100197	100198	100199	100200	100201	100202	100203	100204	100205	100206	100207	100208	100209	100210	100211	100212	100213	100214	100215	100216	100217	100218	100219	100220	100221	100222	100223	100224	100225	100226	100227	100228	100229	100230	100231	100232	100233	100234	100235	100236	100237	100238	100239	100240	100241	100242	100243	100244	100245	100246	100247	100248	100249	100250	100251	100252	100253	100254	100255	100256	100257	100258	100259	100260	100261	100262	100263	100264	100265	100266	100267	100268	100269	100270	100271	100272	100273	100274	100275	100276	100277	100278	100279	100280	100281	100282	100283	100284	100285	100286	100287	100288	100289	100290	100291	100292	100293	100294	100295	100296	100297	100298	100299	100300	100301	100302	100303	100304	100305	100306	10

TABLE 3

The Sorted Distances between Teapot7 and Other Genus Two Models in Teichmüller Space Based on Table 2

Models	Teapot5	Teapot6	Teapot2	Teapot4	Teapot1	Teapot0	Teapot3
distance							
	0.6468	1.1923	3.5202	4.1694	4.1742	4.5179	4.53

Here, we only show the closest ones.

TABLE 4

The Sorted Distances between Pot and Other Genus Two Models in Teichmüller Space Based on Table 2

Distance								
	0.60	0.62	0.63	1.09	5.48	5.88	6.48	8.68

Here, we only show models with maximum and minimum distances to pot model.

TABLE 5

The Sorted Distances between Vase and Other Genus Two Models in Teichmüller Space Based on Table 2

Distance								
	0.53	0.60	0.87	0.90	5.30	5.31	6.32	8.57

Here, we only show models with maximum and minimum distances to pot model.

5.1 Time Complexity

In the whole algorithm pipeline, the most time consuming is computing the hyperbolic uniformization metric. Fig. 9 shows the statistics for the computation of hyperbolic uniformization metric for a closed genus two amphora model with 20k faces. The x -axis indicates the time, and the y -axis indicates the maximal curvature error. The green curve shows the steepest descendant method, and the blue curves show the Newton's method. For most models listed in the work, the time to compute their hyperbolic uniformization metrics is less than 1 minute.

5.2 Robustness

Teichmüller space coordinates are intrinsic properties of surfaces, independent of translation, rotation, scaling, and also insensitive to local noises, and the resolutions of the surface. We tested the robustness of our algorithm by computing for a model with different resolutions. Fig. 10 illustrates one such example. The vase model is tessellated using different resolutions, with the number of faces 5k, 10k,

TABLE 6

The Sorted Distances between Cup and Other Genus Two Models in Teichmüller Space Based on Table 2

Distance								
	1.04	4.72	4.95	5.23	7.46	7.75	7.89	7.92

Here, we only show models with maximum and minimum distances to pot model.

TABLE 7

The Sorted Distances between World Cup and Other Genus Two Models in Teichmüller Space Based on Table 2

Distance								
	0.57	0.76	0.80	1.03	4.30	4.63	5.23	8.31

Here, we only show models with maximum and minimum distances to pot model.

TABLE 8

The Sorted Distances between Teapot3 and Other Genus Two Models in Teichmüller Space Based on Table 2

Distance								
	0.59	0.65	0.73	1.40	4.53	5.16	6.17	8.61

Here, we only show models with maximum and minimum distances to pot model.

20k, and 40k, respectively. We tested our Teichmüller coordinates algorithm on them. The results are listed in Table 1, including the mean average and standard deviation. As we can see, the relative error is less than 0.3 percent.

5.3 Surface Indexing and Classification

Teichmüller coordinates can be directly applied for indexing and classification of surfaces with the same topology. The distance among shapes in the Teichmüller space can be approximated directly using the euclidean distances among their Teichmüller coordinates. In our experiments, we tested genus two closed surfaces and genus three closed surfaces.

For closed genus two surfaces, the dimension of Teichmüller space is seven. The Teichmüller coordinates for eight genus two teapot models are visualized in Fig. 11. The distances in the Teichmüller space among 23 genus two surfaces are listed in Table 2. We cluster the shapes according to their Teichmüller distance. For example, Table 3 shows a neighborhood of the shape of the teapot7

TABLE 9

The Sorted Distances between Eight and Other Genus Two Models in Teichmüller Space Based on Table 2

Distance								
	0.37	0.62	0.96	1.14	5.44	5.67	7.46	8.75

Here, we only show models with maximum and minimum distances to pot model.

model in the Teichmüller space. The surface closest to the teapot7 looks very similar to it. This matches our intuition.

More examples are illustrated in Tables 4, 5, 6, 7, 8, and 9. For each table, we show models with the maximum and minimum distances to example model in Teichmüller space, based on Table 2. Furthermore, by examining Table 2, we can also find that the knotty bottle model (the fifth model of the first row) is farther away from all the others in the Teichmüller space, because its geometry is quite different from the others. Therefore, Teichmüller coordinates match our intuition.

For closed genus three surfaces, the dimension of their Teichmüller space is 13. We visualize the Teichmüller space coordinates for part of those models in Fig. 12. Table 10 lists the distances among those genus three surfaces in the Teichmüller space.

6 CONCLUSION AND FUTURE WORK

In this work, we have proposed a novel approach for surface indexing and classification based on Teichmüller space theory. Teichmüller space is a finite dimensional manifold, where each point represents a conformally equivalent class of surfaces, and a curve represents a deformation process from one shape to another.

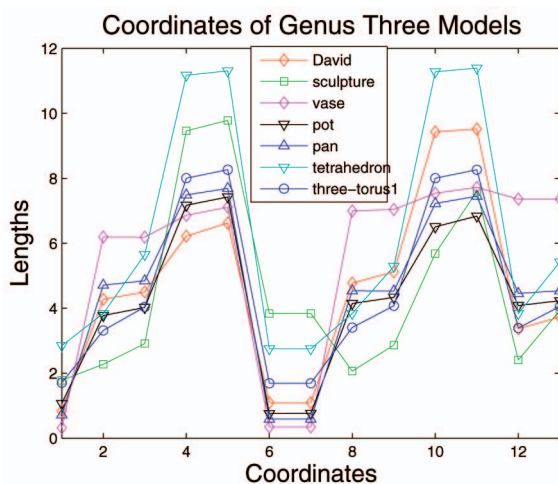


Fig. 12. The dimension of Teichmüller space coordinates for closed genus three surfaces is 13. Here, we visualize the length coordinates of Teichmüller space for part of genus three surfaces listed in Table 10.

TABLE 10

Distances between Genus Three Surfaces in Teichmüller Space

Models	three-torus	tetra-hedron	vase	David	sculp-ture	puppet	pot	pan	clip
	6.43	5.56	13.19	8.16	7.60	8.21	9.19	9.16	5.95
		7.07	8.36	3.89	5.11	2.16	3.02	3.27	8.50
			10.80	8.28	8.82	8.76	9.53	8.73	4.84
				7.29	12.17	7.50	7.03	5.83	12.02
					8.61	3.35	4.45	3.87	9.81
						6.52	6.66	7.49	10.56
							1.47	1.97	9.85
								1.79	10.50
									9.97

As shape descriptors, Teichmüller coordinates are succinct, discriminating and intrinsic, invariant under the rigid motions and scalings, and insensitive to resolutions. Furthermore, the method has solid theoretic foundation, and the computation of Teichmüller coordinates is practical, stable, and efficient.

This work introduces a series of algorithms for computing the Teichmüller coordinates of surfaces with negative Euler numbers. The computational algorithms are theoretically sound and practically simple. The coordinates are algebraically deduced from lengths of geodesic homotopic to a set of special curves under the hyperbolic uniformization metric, which is obtained by using curvature flow method.

We verified our method on a large number of surfaces with negative Euler number and with various geometries, topologies, and resolutions. We apply for surface indexing and classification applications. The extensive experiments demonstrate the efficacy, efficiency, and robustness of our method.

Current work focuses on the computation of Teichmüller coordinates and approximates the geodesic distance between two points in the space by euclidean distance. In theory, Teichmüller space has well-defined Riemannian metrics, and the geodesics between two shapes can be accurately computed. In the future, we will devise practical algorithms to compute the geodesics in Teichmüller spaces, and use geodesic distance to measure the difference between two shapes, to apply for surface deformation and surface morphing.

APPENDIX

Algorithm 1. Compute hyperbolic uniformization metric
for each vertex v_i **do**
 for each face f_{ijk} adjacent to vertex v_i **do**
 compute a radius for v_i :

$$\gamma_i^{jk} = \frac{l_{ki} + l_{ij} - l_{jk}}{2},$$

{ l_{ij} , l_{jk} , l_{ki} : lengths of the edges e_{ij} , e_{jk} , e_{ki} on f_{ijk} }
end for

average the radii from the faces adjacent to v_i :

$$\gamma_i = \frac{1}{m} \sum_{f_{ijk} \in F} \gamma_i^{jk},$$

{ m : the number of the adjacent faces to v_i }

end for

{Associating each vertex with a cone of radius which approximates the original euclidean metric.}

for each edge e_{ij} **do**

compute edge weight $\Phi_{ij}(e_{ij})$ from γ_i , γ_j using hyperbolic cosine law:

$$\cosh l_{ij} = \cosh \gamma_i \cosh \gamma_j + \sinh \gamma_i \sinh \gamma_j \cos \Phi_{ij}$$

end for

{Assigning an edge weight to each edge based on the intersection angle of the two cones centered with the two ending vertices of the edge.}

repeat

for each edge e_{ij} **do**

compute edge length l_{ij} from the current vertices radii γ_i and γ_j , and the fixed edge weight Φ_{ij} using the inverse of hyperbolic cosine law.

end for

{Computing edge length from current circle packing metric.}

for each face f_{ijk} **do**

for all face f_{ijk} **do**

Compute the corner angles θ_i^{jk} from the current edge lengths using hyperbolic cosine law.

end for

end for

for each vertex v_i **do**

Compute the discrete Gaussian curvature K_i on v_i .

if v_i is interior vertex **then**

$$K_i = 2\pi - \sum_{f_{ijk} \in F} \alpha_i^{jk}, \quad (3)$$

{ α_i^{jk} : corner angle attached to vertex v_i in the face f_{ijk} }
else if v_i is boundary vertex **then**

$$K_i = \pi - \sum_{f_{ijk} \in F} \alpha_i^{jk}, \quad (4)$$

end if

end for

for each vertex v_i **do**

Update γ_i of each vertex v_i ,

$$\gamma_i = \gamma_i + \varepsilon(\bar{K}_i - K_i),$$

{ \bar{K}_i : target Gaussian curvature}
end for
until $\max |\bar{K}_i - K_i| < \delta$
{Optimizing discrete hyperbolic Ricci energy with steepest descent method.}

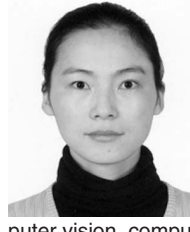
REFERENCES

- [1] W.P. Thurston, *Geometry and Topology of Three-Manifolds*, Princeton lecture notes, 1976.
- [2] M. Seppala and T. Sorvali, *Geometry of Riemann Surfaces and Teichmüller Spaces*, North-Holland Math. Studies, 1992.
- [3] X. Gu and S.-T. Yau, "Global Conformal Parameterization," *Proc. Symp. Geometry Processing (SGP '03)*, pp. 127-137, 2003.
- [4] X. Gu and B.C. Vemuri, "Matching 3D Shapes Using 2D Conformal Representations," *Proc. Seventh Int'l Conf. Medical Image Computing and Computer Assisted Intervention (MICCAI '04)*, pp. 771-780, 2004.
- [5] Y. Wang, M. Chiang, and P.M. Thompson, "Mutual Information-Based 3D Surface Matching with Applications to Face Recognition and Brain Mapping," *Proc. 10th IEEE Int'l Conf. Computer Vision (ICCV '05)*, vol. 1, pp. 527-534, 2005.
- [6] S. Wang, Y. Wang, M. Jin, X. Gu, and D. Samaras, "3D Surface Matching and Recognition Using Conformal Geometry," *Proc. IEEE Conf. Computer Vision and Pattern Recognition (CVPR '06)*, pp. 2453-2460, 2006.
- [7] M. Jin, F. Luo, S.-T. Yau, and X. Gu, "Computing Geodesic Spectra of Surfaces," *Proc. ACM Symp. Solid and Physical Modeling (SPM '07)*, pp. 387-393, 2007.
- [8] X. Gu and S.-T. Yau, "Surface Classification Using Conformal Structures," *Proc. Ninth IEEE Int'l Conf. Computer Vision (ICCV '03)*, pp. 701-708, 2003.
- [9] F. Luo, "Geodesic Length Functions and Teichmüller Spaces," *J. Differential Geometry*, vol. 48, p. 275, 1998.
- [10] R.S. Hamilton, "The Ricci Flow on Surfaces," *Math. General Relativity*, vol. 71, pp. 237-262, 1988.
- [11] B. Chow and F. Luo, "Combinatorial Ricci Flows on Surfaces," *J. Differential Geometry*, vol. 63, no. 1, pp. 97-129, 2003.
- [12] P. Buser, *Geometry and Spectra of Compact Riemann Surfaces*. Birkhäuser, 1992.
- [13] W.P. Thurston, *Three-Dimensional Geometry and Topology*. Princeton Univ. Press, 1997.
- [14] J.R. Munkres, *Elements of Algebraic Topology*. Addison-Wesley, 1984.
- [15] J.W. Tangelder and R.C. Veltkamp, "A Survey of Content Based 3D Shape Retrieval Methods," *Multimedia Tools and Applications*, in press, 2008.
- [16] C. Carner, M. Jin, X. Gu, and H. Qin, "Topology-Driven Surface Mappings with Robust Feature Alignment," *Proc. IEEE Visualization Conf.*, pp. 543-550, 2005.
- [17] N. Iyer, S. Jayanti, K. Lou, Y. Kalyanaraman, and K. Ramani, "Three-Dimensional Shape Searching: State-of-the-Art Review and Future Trends," *Computer-Aided Design*, vol. 37, no. 5, pp. 509-530, 2005.
- [18] X. Gu, S. Wang, J. Kim, Y. Zeng, Y. Wang, H. Qin, and D. Samaras, "Ricci Flow for 3D Shape Analysis," *Proc. 11th IEEE Int'l Conf. Computer Vision (ICCV '07)*, pp. 1-8, 2007.
- [19] R.-M. Rustamov, "Laplace-Beltrami Eigenfunctions for Deformation Invariant Shape Representation," *Proc. Symp. Geometry Processing (SGP)*, 2007.
- [20] M. Reuter, F.-E. Wolter, and N. Petnecke, "Laplace-Spectra as Fingerprints for Shape Matching," *Proc. ACM Symp. Solid and Physical Modeling (SPM '05)*, pp. 101-106, 2005.
- [21] P. Xiang, C.-O. Hua, F.-X. Gang, and Z.-B. Chuan, "Pose Insensitive 3D Retrieval by Poisson Shape Histogram," *Lecture Notes in Computer Science*, vol. 4488, pp. 25-32, 2007.
- [22] V. Jain and H. Zhang, "A Spectral Approach to Shape-Based Retrieval of Articulated 3D Models," *Computer Aided Design*, vol. 39, pp. 398-407, 2007.
- [23] M. Ben-Chen and C. Gotsman, "Characterizing Shape Using Conformal Factors," *Proc. Eurographics Workshop Shape Retrieval*, 2008.
- [24] K. Stephenson, *Introduction to Circle Packing*. Cambridge Univ. Press, 2005.

- [25] A. Elad and R. Kimmel, "On Bending Invariant Signatures for Surfaces," *IEEE Trans. Pattern Analysis and Machine Intelligence*, vol. 25, no. 10, pp. 1285-1295, Oct. 2003.
- [26] T. Tung and F. Schmitt, "The Augmented Multiresolution Reeb Graph Approach for Content-Based Retrieval of 3D Shapes," *Int'l J. Shape Modeling*, vol. 11, no. 1, pp. 91-120, 2005.
- [27] R. Gal, A. Shamir, and D. Cohen-Or, "Pose Oblivious Shape Signature," *IEEE Trans. Visualization and Computer Graphics*, vol. 13, no. 2, pp. 261-271, Mar./Apr. 2007.
- [28] P. Shilane, P. Min, M. Kazhdan, and T. Funkhouser, "The Princeton Shape Benchmark," *Proc. IEEE Int'l Conf. Shape Modeling Int'l (SMI '04)*, pp. 167-178, 2004.
- [29] R.S. Hamilton, "Three Manifolds with Positive Ricci Curvature," *J. Differential Geometry*, vol. 17, pp. 255-306, 1982.
- [30] B. Chow, P. Lu, and L. Ni, "Hamilton's Ricci Flow," *Am. Math. Soc.*, vol. 77, 2006.
- [31] B. Chow, S.-C. Chu, D. Glickenstein, C. Guenther, J. Isenberg, F. Luo, T. Ivey, D. Knopf, P. Lu, and L. Ni, "The Ricci Flow: Techniques and Applications. Part I: Mathematical Surveys and Monographs," *Am. Math. Soc.*, vol. 135, 2007.
- [32] C. de Verdiere Yves, "Un Principe Variationnel pour les Empilements de Cercles," *Inventiones Math.*, vol. 104, no. 3, pp. 655-669, 1991.
- [33] Braegger and Walter, "Kreispackungen und Triangulierungen," *Enseign. Math.*, vol. 2(38), no. 3-4, pp. 201-217, 1992.
- [34] I. Rivin, "Euclidean Structures on Simplicial Surfaces and Hyperbolic Volume," *Ann. Math.*, vol. 2, no. 3, pp. 553-580, 1994.
- [35] F. Luo, "Combinatorial Yamabe Flow on Surfaces," *Comm. Contemporary Math.*, vol. 6, no. 5, pp. 765-780, 2004.
- [36] F. Luo, *On Teichmüller Space of Surface with Boundary*, preprint, 2005.
- [37] G. Perelman, "The Entropy Formula for the Ricci Flow and Its Geometric Applications," technical report arXiv.org, Nov. 2002.
- [38] G. Perelman, "Ricci Flow with Surgery on Three-Manifolds," technical report arXiv.org, Mar. 2003.
- [39] G. Perelman, "Finite Extinction Time for the Solutions to the Ricci Flow on Certain Three-Manifolds," technical report arXiv.org, July 2003.
- [40] G. Leibon, "Characterizing the Delaunay Decompositions of Compact Hyperbolic Surfaces," *Geometry and Topology*, vol. 6, pp. 361-391, 2002.
- [41] A.I. Bobenko and B.A. Springborn, "Variational Principles for Circle Patterns and Koebe's Theorem," *Trans. Am. Math. Soc.*, vol. 256, no. 2, pp. 659-689, 2004.
- [42] M. Jin, J. Kim, F. Luo, and X. Gu, "Discrete Surface Ricci Flow," *IEEE Trans. Visualization and Computer Graphics*, vol. 14, no. 5, Sept./Oct. 2008.
- [43] L. Kharevych, B. Springborn, and P. Schröder, "Discrete Conformal Mappings via Circle Patterns," *ACM Trans. Graphics*, vol. 25, no. 2, pp. 412-438, 2006.
- [44] M. Ben-Chen, C. Gotsman, and G. Bunin, "Conformal Flattening by Curvature Prescription and Metric Scaling," *Computer Graphics Forum (Proc. Eurographics '08)*, vol. 27, no. 2, 2008.
- [45] Y.-L. Yang, J. Kim, F. Luo, and X. Gu, "Optimal Surface Parameterization Using Inverse Curvature Map," *IEEE Trans. Visualization and Computer Graphics*, vol. 14, no. 5, pp. 1054-1066, Sept./Oct. 2008.
- [46] A.I. Bobenko and B.A. Springborn, "Variational Principles for Circle Patterns and Koebe's Theorem," *Trans. Am. Math. Soc.*, vol. 356, pp. 659-689, 2004.
- [47] A. Bobenko and P. Schröder, "Discrete Willmore Flow," *Proc. Symp. Geometry Processing (SGP '05)*, pp. 101-110, 2005.
- [48] Y.C. de Verdière, "Un Principe Variationnel pour les Empilements de Cercles. [a Variational Principle for Circle Packings]," *Invent. Math.*, vol. 104, no. 3, pp. 655-669, 1991.
- [49] P.L. Bowers and M.K. Hurdal, "Planar Conformal Mappings of Piecewise Flat Surfaces," *Visualization and Math. III*, pp. 3-34, Springer, 2003.
- [50] B. Springborn, P. Schröder, and U. Pinkall, "Conformal Equivalence of Triangle Meshes," *Proc. ACM SIGGRAPH*, 2008.
- [51] M.S. Floater and K. Hormann, "Surface Parameterization: A Tutorial and Survey," *Advances in Multiresolution for Geometric Modelling*, pp. 157-186, Springer, 2005.
- [52] A. Sheffer, E. Praun, and K. Rose, "Mesh Parameterization Methods and Their Applications," *Foundations and Trends in Computer Graphics and Vision*, vol. 2, no. 2, 2006.



Miao Jin received the PhD degree in computer science from Stony Brook University in 2008. She is an assistant professor in the Center for Advanced Computer Studies, University of Louisiana, Lafayette. Her research interests include computer graphics and computer vision. Her major works include computational conformal geometry, computing surface geometric structures, and shape space.



Wei Zeng received the BS and MS degrees in computer science from Shandong University of China in 2003 and 2005, respectively. She is a PhD candidate in the Institute of Computing Technology, Chinese Academy of Sciences. She is a visiting scholar in the Department of Computer Science, Stony Brook University, Stony Brook, New York. Her research interests include computational conformal geometry, computer vision, computer graphics, and shape analysis.



Feng Luo received the PhD degree from the University of California at San Diego in 1989. He is a professor of mathematics in the Department of Mathematics, Rutgers University, Piscataway, New Jersey. His research interests include geometry and topology on surfaces and 3-manifolds, and computer graphics.



Xianfeng Gu received the PhD degree in computer science from Harvard University in 2003. He is an assistant professor of computer science in the Department of Computer Science, Stony Brook University, Stony Brook, New York. His research interests include computer graphics, computer vision, and medical imaging. His major works include geometry images, global conformal surface parameterization, manifold splines, and computational conformal geometry. He won the US National Science Foundation CAREER award in 2004. He is a member of the IEEE and the IEEE Computer Society.

▷ For more information on this or any other computing topic, please visit our Digital Library at www.computer.org/publications/dlib.